ENERGY SPECTRA OF RADIOACTIVE NEUTRON SOURCES

H.PAUW

ENERGY SPECTRA OF RADIOACTIVE NEUTRON SOURCES

ACADEMISCH PROEFSCHRIFT

ter verkrijging van de graad van doctor in de wiskunde
en natuurwetenschappen aan de Universiteit van Amsterdam
op gezag van de rector magnificus Mr. A.D. Belinfante,
hoogleraar in de faculteit der rechtsgeleerdheid,
in het openbaar te verdedigen in de aula der Universiteit
(tijdelijk in de Lutherse Kerk, ingang Singel 411, hoek Spui)
op woensdag 25 november 1970 te 16.00 uur

door

HERMANUS PAUW
geboren te Edam

1970

Drukkerij JOKO Amsterdam

Promotor: Prof. Dr. A.H.W. Aten Jr.

Coreferent: Prof. Dr. J.J. van Loef

The work described in this thesis is part of the research program of the Institute for Nuclear Research (I.K.O.), made possible by financial support from the Foundation for Fundamental Research on Matter (F.O.M.) and the Netherlands Organization for the Advancement of Pure Research (Z.W.O.).

Aan mijn ouders
Aan mijn vrouw

VOORWOORD

Gaarne maak ik van de gelegenheid gebruik allen te danken die hebben bijgedragen tot mijn wetenschappelijke vorming en aan het tot stand komen van dit proefschrift.

Hooggeleerde Aten, hooggeschatte promotor, Uw persoonlijke belangstelling voor neutronen is voor mij een stimulans geweest dit onderzoek te voltooien. Ik heb het steeds bijzonder gewaardeerd, dat het mogelijk is gebleken onder Uw leiding volgens mijn eigen inzichten te kunnen werken.

Hooggeleerde van Loef, U wil ik gaarne dankzeggen voor het kritisch doorlezen van het manuscript.

Dank ben ik verschuldigd aan vele medewerkers van het I.K.O., die in de afgelopen jaren op enigerlei wijze mij van dienst zijn geweest. Ik denk dan vooral aan het personeel van de tekenkamer en de werkplaats voor het ontwerpen en vervaardigen van apparatuur. Voor de nauwgezette uitvoering van de figuren ben ik zeer erkentelijk.

Alle medewerkers van de chemische afdeling dank ik voor de bijzonder prettige samenwerking. Vooral Dr. P.W.F. Louwrier en Drs. B.J. Mijnheer, die hun kostbare tijd hebben besteed aan het nauwgezet doorlezen van de tekst. Ben, jouw aanwijzingen zijn voor mij altijd een grote steun geweest.

Mijn speciale dank gaat uit naar Elly van der Hauten voor het uitvoeren van de experimenten en het verrichten van de soms schijnbaar eindeloze hoeveelheid rekenwerk.

Voorts wil ik ook Mevrouw M. Oskam - Tamboezer bedanken voor het persklaar maken van het manuscript.

CONTENTS

INTRODUCTION

The main purpose of our investigation was to solve the various discrepancies concerning the neutron intensity and neutron spectrum of different kinds of $^{9}Be(\alpha,n)$ neutron sources below 1.5 MeV.

For neutron purposes it is essential to know what fraction of the total number of neutrons have energies below about 1.5 MeV.

Because of the fact that the neutron is an electrically neutral particle, we cannot detect it directly by means of electrical and magnetic fields as is possible with α- and β-particles, protons and electrons.
Indirect detection methods must be used for the observation and measurement of neutrons.

By interaction with nuclei, neutrons produce secondary charged particles or radioactive isotopes, either of which can be detected and measured in a quantitative way. If the reaction cross section is accurately known and if the number of nuclear reactions is determined, the neutron intensity can be calculated. Neutron detectors make use of such indirect methods. The neutron energy is normally measured by means of a neutron spectrometer.

However, the disadvantage of almost all of these instruments is that neutrons with an energy below 1.5 MeV are difficult to detect, because the sensitivity for γ-ray radiation becomes too high, relative to that for neutrons. For this reason we have used simple neutron detectors, which are insensitive to γ-rays.

One of the neutron detectors was based on a principle used extensively by Heertje (He 63), which consists of the fact that every (n,γ) activation detector is in principle a suitable artificial threshold detector when surrounded by a layer of ^{10}B. Such a detector is particularly useful in the

energy region below 1.5 MeV. We have used such a hollow ^{10}B sphere for activating gold and indium.

For the calculations, which are fully explained in Chapter II, accurate neutron reaction cross section curves are required. It will be shown in Chapter III that the gold and indium cross section curves are at present well known.

The calibration of the gold and indium activation detectors will be discussed in Chapter IV.

Besides gold and indium, we have also made use of thin layers of neptunium, plutonium and uranium in combination with plastic foils, which record the fission products as small tracks. In Chapter V the use and the calibration of the fission track registration method are explained.

Both types of neutron detectors were used to obtain more detailed information concerning the neutron intensity and average spectrum of different kinds of $^{9}Be(\alpha,n)$ neutron sources and of a ^{252}Cf neutron source below 1.5 MeV. The same technique was also used to study the energy spectra of some other types of neutron sources.

The spectra of the neutron sources, used in this laboratory, are discussed in Chapter I, while Chapter VI shows the experimental results in relation to other experiments and theoretical expectations.

CHAPTER I

NEUTRON SOURCES

Radioactive neutron sources are used for a variety of experiments. The dimensions and other characteristics of those sources which are used most frequently, are shown in table I.1. (The anisotropy factor is a correction factor for the fact that the neutron emission in the direction perpendicular to the cylindrical axis of the source is higher than the average neutron output per steradian.)

For the ^{9}Be(α,n) sources and the ^{252}Cf neutron source, we have tried to obtain more detailed information concerning the neutron intensity and spectrum below 1.5 MeV with the help of activation detectors (gold and indium), and neutron fission detectors (plutonium, neptunium and uranium). Both kinds of neutron detectors were also used to obtain more information about the complete spectrum of the ^{241}AmLi and ^{241}AmAl neutron sources.

The energy spectra of these sources, published by different authors, are described in this chapter.

^{9}Be(α,n) neutron sources: ^{241}AmBe, ^{239}PuBe, ^{226}RaBe, ^{242}CmBe.

A normal ^{9}Be(α,n) neutron source contains a mixture of an α-emitting nuclide with the light element ^{9}Be. It is essential to combine the α-emitter with a light (low Z) element since the energy of the α-particles must be sufficiently high to penetrate the potential (Coulomb) barrier around the nucleus. It is possible to obtain neutrons from aluminium or lithium (or their compounds or alloys) by α-irradiation, but the neutron emission rate of such sources is much smaller for the same number of millicuries mixed with beryllium.

Table I.1 The neutron sources used in our experiments.

Source	Approx. amount of radioactive material in Ci	Material of container	Dimensions in mm height	diameter	Manufacturer	Approx. neutron emission rate in n/sec	Anisotropy factor
^{241}AmBe	3	stainless steel	48.5	22.4	R.C.A.*	8.6×10^{6}	1.039
^{239}PuBe	5	tantalum, stainless steel	52.3	39.5	NUMEC	1.0×10^{7}	1.052
^{226}RaBe	0.1	monel, platinum	15.4	15.0	Union Minière	1.5×10^{6}	1.014
^{242}CmBe	1	stainless steel	19.4	17.4	R.C.A.	3.5×10^{6}	1.012
Mock-Fission	1	stainless steel	17.0	15.0	R.C.A.		
^{252}Cf	8×10^{-4}	monel	15.0	15.0	Euratom/IKO	3.5×10^{6}	1.019
^{241}AmLi	1.5	stainless steel	31.0	22.4	R.C.A.	6.7×10^{4}	1.023
^{241}AmAl	5	aluminium	72.0	12.0	Euratom	4.4×10^{4}	1.042
^{124}SbBe	1	aluminium	36.0	23.0	R.C.A.	1.0×10^{6}	1.030
^{124}SbBe		titanium					1.105

* The Radiochemical Centre Amersham

We are grateful to Mijnheer (Mij 70), who measured the neutron emission rates and the anisotropy factors.

Traditionally, (α,n) sources have consisted of radium (plus daughters), or polonium in intimate mixture with beryllium. Of late these sources have, however, become old-fashioned, since α-emitting transuranium isotopes are now becoming available in quantity.

Sources prepared from ^{241}Am, ^{239}Pu and ^{242}Cm have several advantages, such as freedom from high intensity gamma-rays. The transuranium elements form intermetallic compounds with beryllium, whereas in the case of radium it is necessary to prepare pressed mechanical mixtures. However, only the $^{239}PuBe$ source actually consists of an intermetallic compound of ^{239}Pu and ^{9}Be.

The neutron yield, the maximum neutron energy and certain other characteristics of the (α,n) reaction are given in Table I.2.

In Table I.3 the neutron emission rates have been given for different target elements. These data have been taken from Arnold (Ar 68) and have been calculated for ideal circumstances.

In principle $^{9}Be(\alpha,n)$ neutron spectrum calculations should be based on (α,n) cross section values combined with the correct angular distribution function. Cross section measurements show that the neutron emission from the $^{9}Be(\alpha,n)$ reaction occurs as a series of broad overlapping resonances in the compound nucleus ^{13}C and that the neutron spectrum is due to neutrons leaving ^{12}C in the ground state, the 4.43 MeV state and the 7.66 MeV state respectively. However, Verbinski (Ve 68) has determined that part of the neutron spectrum is due to other reactions, competing with those mentioned, such as:

$$^{9}Be(\alpha,\alpha')^{9}Be^{*} \rightarrow {}^{8}Be + n,$$
$$^{9}Be(\alpha,{}^{8}Be)^{5}He \rightarrow {}^{4}He + n \text{ and}$$
$$^{9}Be(\alpha,n)3\alpha,$$

which have much smaller Q-values than the $^{9}Be(\alpha,n)^{12}C$ reac-

Table I.2 Some characteristics of the $^{9}Be(\alpha,n)$ neutron sources.

source	kind of mixture	α-energy (MeV)	maximum neutron energy (MeV)	neutron emission rate in n/s/αCurie
$^{241}AmBe$	pelleted mixture of Am-oxide + Be	5.48	11.0	2.7×10^{6}
$^{239}PuBe$	alloy of Pu + Be	5.15	10.7	2.2×10^{6}
$^{226}RaBe$*	pressed mechanical mixture of Ra + Be	4.78-7.69	13.1	2.0×10^{7}
$^{242}CmBe$	pelleted mixture of Cm-oxide + Be	6.11	11.8	7.0×10^{6}

* The $^{226}RaBe$ neutron source contains all the daughters of ^{226}Ra, however ^{210}Po will not normally be in equilibrium with ^{226}Ra. The α-energy of 7.69 MeV is from the ^{226}Ra-daughter ^{214}Po.
For the neutron emission rate it is assumed that all the daughters of ^{226}Ra have grown in.
The calculation of the maximum neutron energy was based on a Q-value of 5.65 MeV for the $^{9}Be(\alpha,n)^{12}C$ reaction.

Table I.3 The (α,n) emission from mixtures of ^{241}Am and light elements.

target element	maximum neutron energy (MeV)	neutron emission rate in n/s/αCurie
Be	11.0	2.7×10^{6}
O	5.8	2.0×10^{3}
Al	2.5	2.7×10^{4}
Li	1.5	9.8×10^{4}

tion.

The calculated neutron peak from these accompanying reactions lies around 300 keV (Ro 62), and provides the main neutron contribution below 1.5 MeV.

Earlier neutron spectrum calculations by Hess (He 59) and Notarrigo (No 62), in which it was assumed that the neutrons leaving ^{12}C in the different states, have isotropic angular distributions, provided only a very crude approximation to the actual spectrum. Later calculations by Anderson (An 63), which did not involve the assumption of isotropic angular distribution, resulted in better agreement with experimental data. However, the major peak at 3.2 MeV was only weakly suggested by these calculations.

This problem was solved by Van der Zwan (Zw 68), who paid more attention to the neutrons emitted in the backward direction with respect to the incident α-particle. Neutron spectra for ^{241}AmBe and ^{239}PuBe sources calculated in this way are in very good agreement with the measured ones.

The fact that one has to pay more attention to the neutrons emitted in the backwards direction was proved by Geiger (Ge 70a). In these experiments a thick Be-target was irradiated with a 5.48 MeV α-beam. After appropriate weighting and summation of the neutron spectra taken with a stilbene neutron spectrometer at 15^{o} intervals, the simulated ^{241}AmBe source spectrum was obtained. This spectrum was in excellent agreement with the one obtained directly from a ^{241}AmBe source and with spectra published by other authors. It is interesting to note that the two principal peaks in the composite spectrum at 3.4 and 5.0 MeV are caused by intense peaking in the backward and forward direction. The 5.0 MeV peak seems to be composed of three neutron peaks, with components at approximately 4.4 and 5.0 MeV and a shoulder at 5.7 MeV, due to neutrons emitted from the 4.43 MeV ^{12}C state.

The numerical graphical analysis of Lehman (Le 68), based on published differential and integral cross sections

for the $^{9}Be(\alpha,n)$ reaction agrees with the results, obtained by Van der Zwan (Zw 68) and Geiger (Ge 70a).

Equally good results were obtained in recent calculations of Notarrigo (No 69), which also took account of the anisotropy.

However, it has not yet been possible to include in the calculations the contributions from the minor reactions mentioned, which don't lead to ^{12}C and the effects due to neutron reactions in the source itself:

$^{9}Be(n,n')^{9}Be^{*}$,
$^{9}Be(n,2n)^{8}Be$ and
$^{239}Pu(n,f)$ for PuBe sources.

The results of calculations by Van der Zwan (Zw 68) for ^{241}AmBe and ^{239}PuBe neutron sources are shown in figure I.1 and figure I.2, together with different measured spectra of sources for which the neutron intensity and neutron spectrum below 1.5 MeV were determined in our experiments.

Because the α-energies of ^{241}Am and of ^{239}Pu are very similar, the differences between the spectra of ^{241}AmBe and of ^{239}PuBe sources must be quite small.

Because in the ^{226}RaBe source the α-energies of the ^{226}Ra with all of its descendants range from 4.8 to 7.7 MeV, and because of the $^{9}Be(\gamma,n)^{8}Be$ reaction, the peaks in the ^{226}RaBe spectrum are not as well defined as those for the other $^{9}Be(\alpha,n)$ spectra.

Different ^{226}RaBe neutron spectra are shown in figure I.3

In Table I.4 the theoretical energies of the predominant peaks are given for a ^{239}PuBe source, calculated by Lehman (Le 68), Van der Zwan (Zw 68) and Notarrigo (No 69).

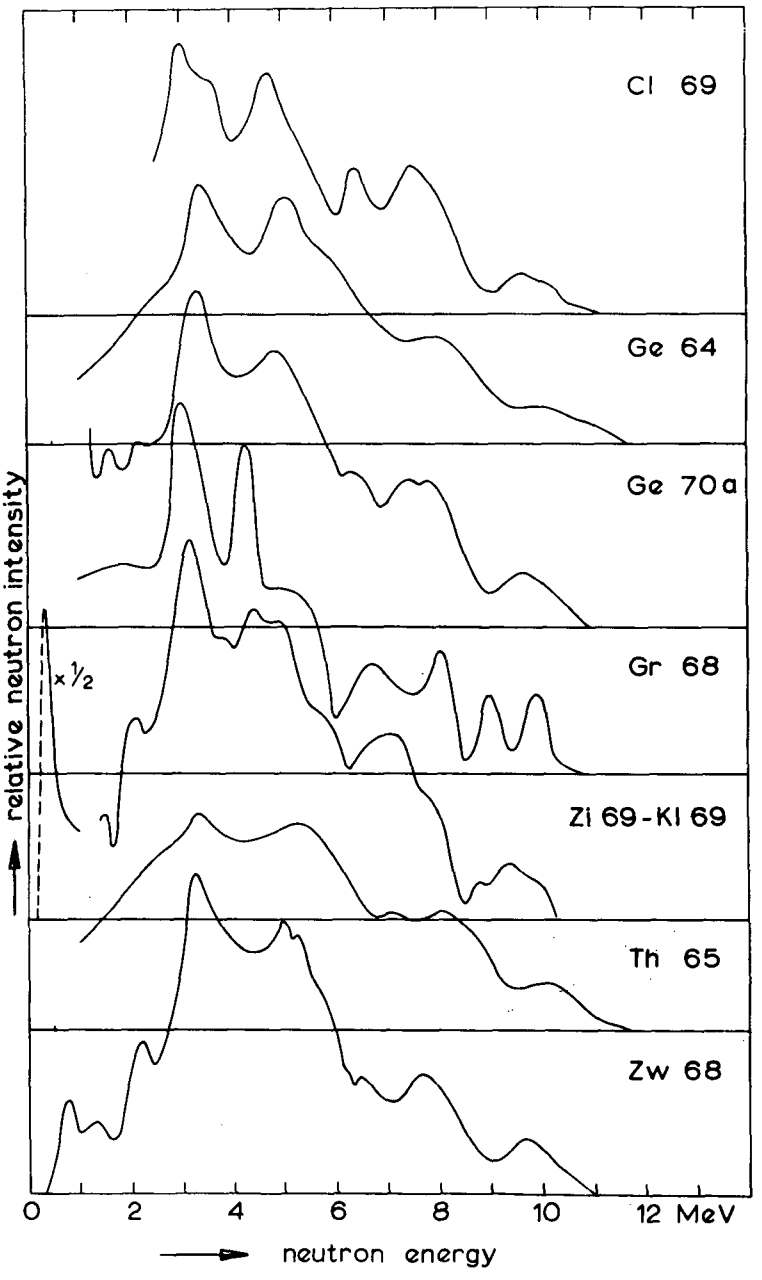

Fig. I.1 Neutron energy spectra of ^{241}AmBe sources

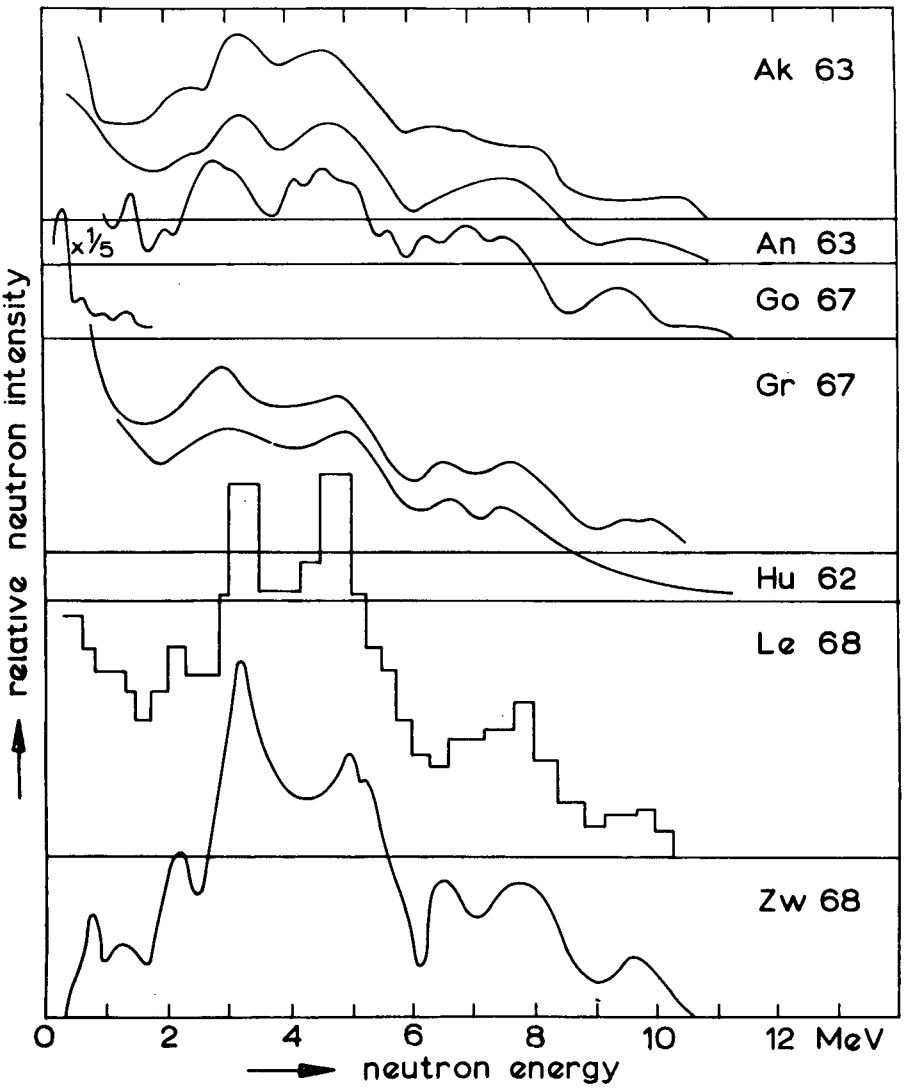

Fig. I.2 Neutron energy spectra of ^{239}PuBe sources

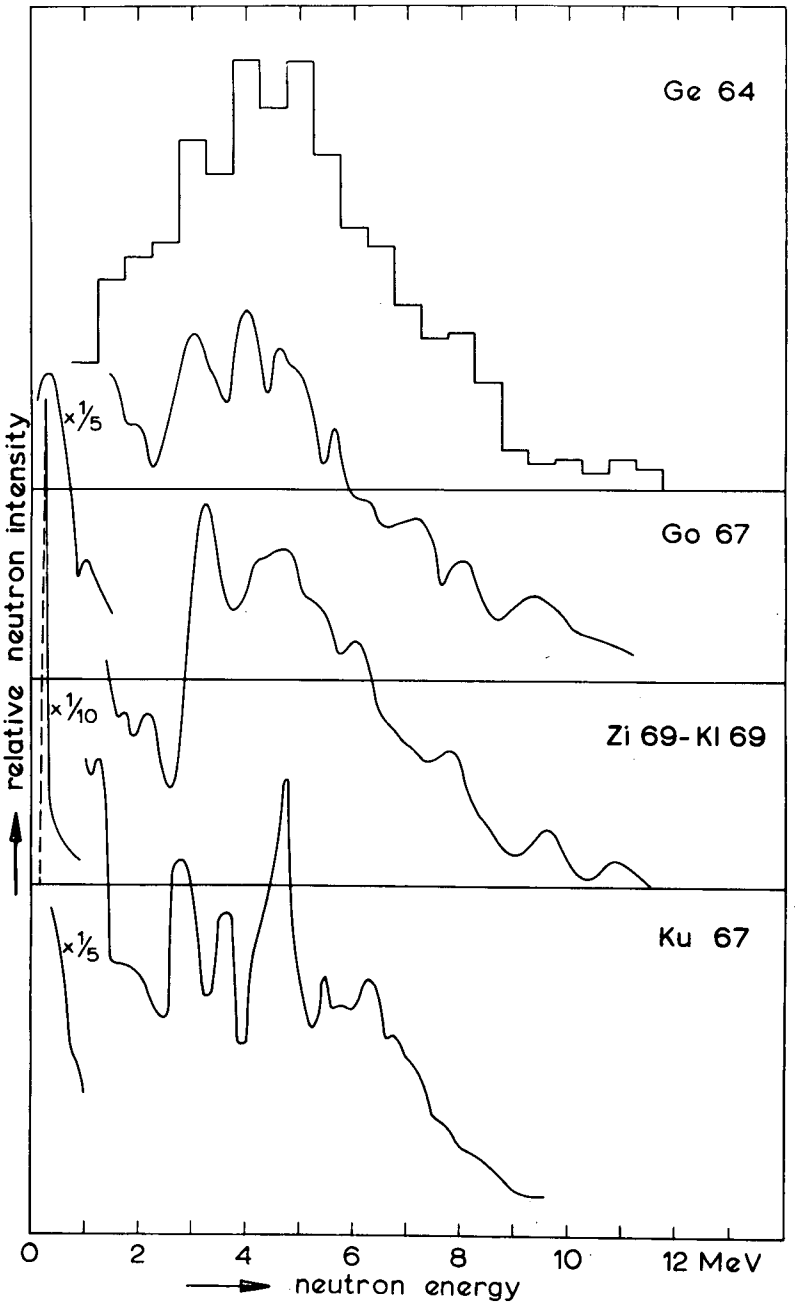

Fig. I.3 Neutron energy spectra of ^{226}RaBe sources

Table I.4 The theoretical neutron energies of the predominant peaks for a ^{239}PuBe source.

Literature											
Le 68	0.54	0.78	1.1	1.4	2.3	3.2	4.8	5.6	6.7	7.8	9.8
No 69						3.2	4.8	5.6	6.4	7.8	9.7
Zw 68		0.75		1.20	2.10	3.15	4.95	5.60	6.50	7.75	9.65

From theory it is expected that all ^{9}Be(α,n) sources show these neutron peaks. The position of the theoretically calculated neutron peaks above 1.5 MeV are in good agreement with several measured results. Below 1.5 MeV only very few measurements are known, because most neutron spectrometers are sensitive to γ-rays and cannot be used for these sources in this energy range.

The spectral measurements of Goryachev (Go 67) (^{210}PoBe, ^{239}PuBe, ^{226}RaBe) and of Kukhtevich (Ku 67) (^{210}PoBe, ^{226}RaBe) actually show small neutron peaks at about 1.4, 1.1, 0.8 and 0.3 MeV, in agreement with theoretical expectations. However, in their spectra the predominant peak at 4.8 MeV has been resolved into three neutron peaks, with components at approximately 4.0 and 4.7 MeV and a shoulder at 5.2 MeV, which to a certain extent can also be seen in the ^{241}AmBe spectrum of Geiger (Ge 70a).

The results of Zill (Zi 69) for ^{241}AmBe and ^{226}RaBe sources below 1 MeV only show a clear neutron peak at - or below - about 0.3 MeV, but none at 0.7 MeV.

Because our ^{241}AmBe and ^{242}CmBe neutron sources contain a pelleted mixture of the target element beryllium and the oxide of the radioisotope, it is to be expected that the (α,n) reaction on oxygen will contribute to the neutron spectrum. However, from Table I.3 it can be seen that the contribution amounts to only about one part in a thousand, and may therefore be neglected.

As described above several secondary reactions occur inside the neutron source itself. For example the scattering of neutrons will increase with the size of the source.

Anderson (An 68) showed that in the case of different size ^{239}PuBe sources the average neutron energy decreased as the source size increased. However, for different sizes the neutron spectrum above about 2 MeV remained essentially the same. Only the number of neutrons below about 2 MeV will increase as the source size increases, due to the above mentioned neutron reactions within the source.
Thus the results obtained by us, which are described in detail in chapter VI, are valid only for neutron sources of this type and construction used by us.

A ^{242}CmBe neutron source spectrum, measured by Lorch (Lo 70) is shown in figure I.4.

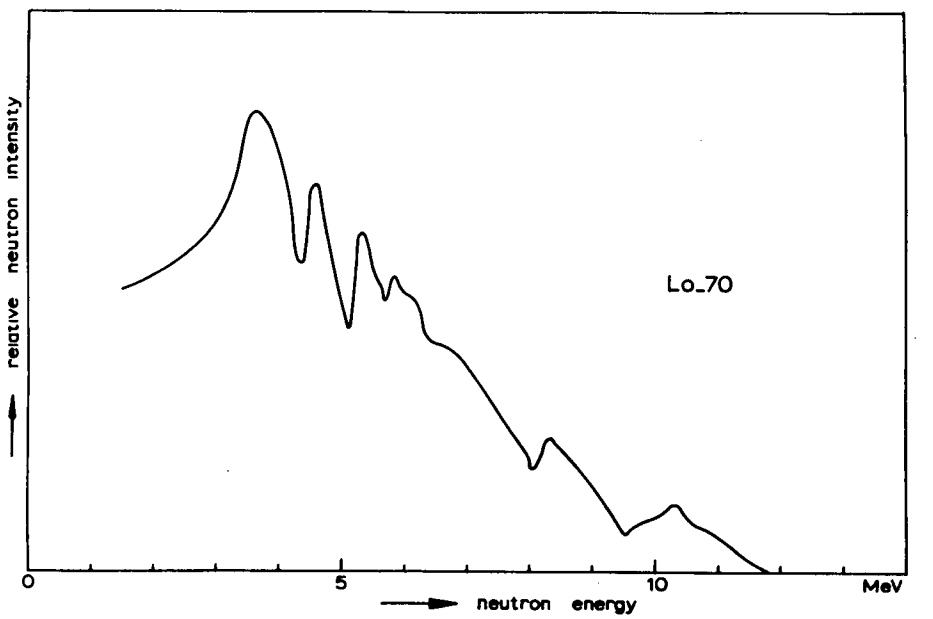

Fig. I.4 Neutron energy spectrum of a ^{242}CmBe source

It is surprising that the ^{242}CmBe neutron spectrum is very different from what is expected on the basis of our knowledge concerning ^{239}PuBe and ^{241}AmBe sources. The predominant neutron peaks are hardly resolved and the relative intensities of the neutron peaks are different from those known from other ^{9}Be(α,n) sources. The 4.8 MeV peak, normally represented in ^{9}Be(α,n) spectra as a single peak, consists of three peaks in the ^{242}CmBe spectrum with components at approximately 4.6 MeV, 5.3 MeV and 6.0 MeV. The position of the neutron peaks in the ^{242}CmBe spectrum is rather similar to the ^{9}Be(α,n) neutron spectra of Goryachev (Go 67) and Kukhtevich (Ku 67). There is also a strange peak at approximately 10.5 MeV.

Lorch has confirmed the shape of the ^{242}CmBe spectrum by a large number of runs on the same source. With the same equipment he measured an ^{241}AmBe spectrum, which shows the well-known sharp double peak at approximately 3.6 MeV and 5.4 MeV, in agreement with other measured ^{241}AmBe spectra. To a certain extent the ^{242}CmBe spectrum resembles a fission spectrum, which probably means that the source contains a certain amount of fissile material. However, the contribution of spontaneous fission to the neutron production should be negligible in ^{242}CmBe sources.

The Mock-Fission neutron source: ^{210}Po + Be + B + F.

The energy of the ^{210}Po α-particle is 5.30 MeV.

The characteristics of the ^{210}Po(α,n) reactions with light elements are shown in table I.5 (once more for ideal circumstances).

A mixture of ^{210}Po, Be, B, F (and Li) in the correct proportions constitutes a neutron source, the spectrum of which resembles an uranium fission spectrum.

The individual ^{10}B(α,n), ^{19}F(α,n) and ^{6}Li(α,n) neutron spectra are shown in figure I.5.

Table I.5 The (α,n) emission from mixtures of ^{210}Po and light elements.

target element	maximum neutron energy (MeV)	neutron emission rate in n/s/α Curie
Be	10.8	2.8×10^6
B	6.4	8.1×10^5
F	2.6	3.7×10^5
Li	1.4	9.0×10^4

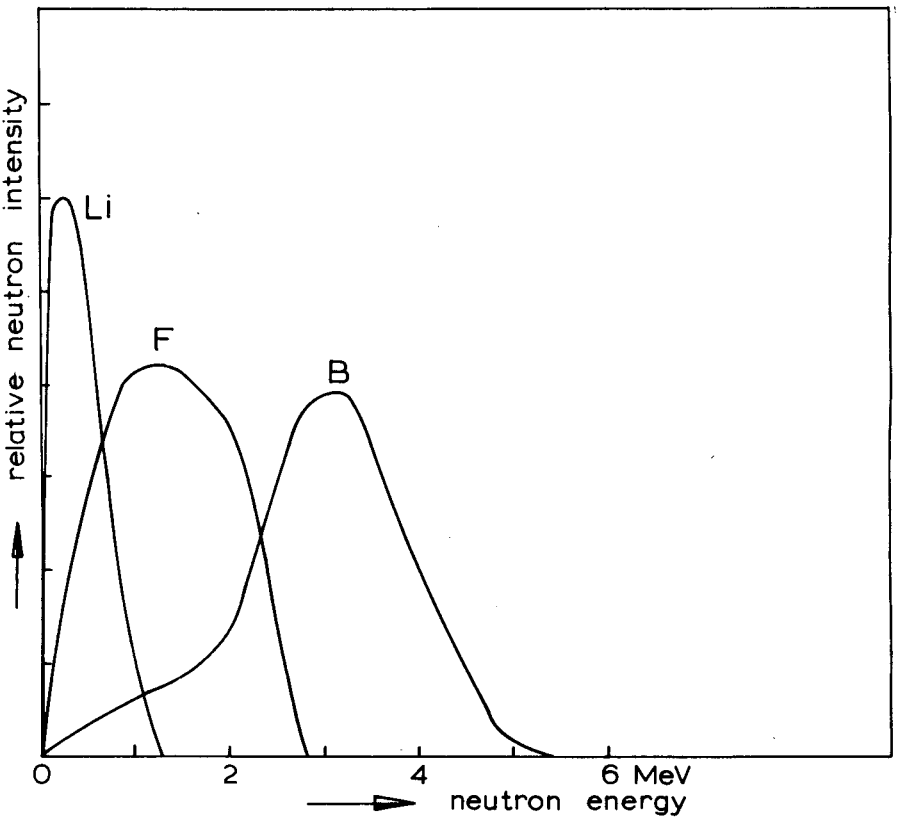

Fig. I.5 Theoretical neutron spectra from ^{210}Po alphas and thick Li, B and F targets (He 59).

The only measured Mock-Fission spectrum was published by Tochilin (To 58). He determined the neutron energy spectra for three different mixtures. The results are shown in figure I.6.

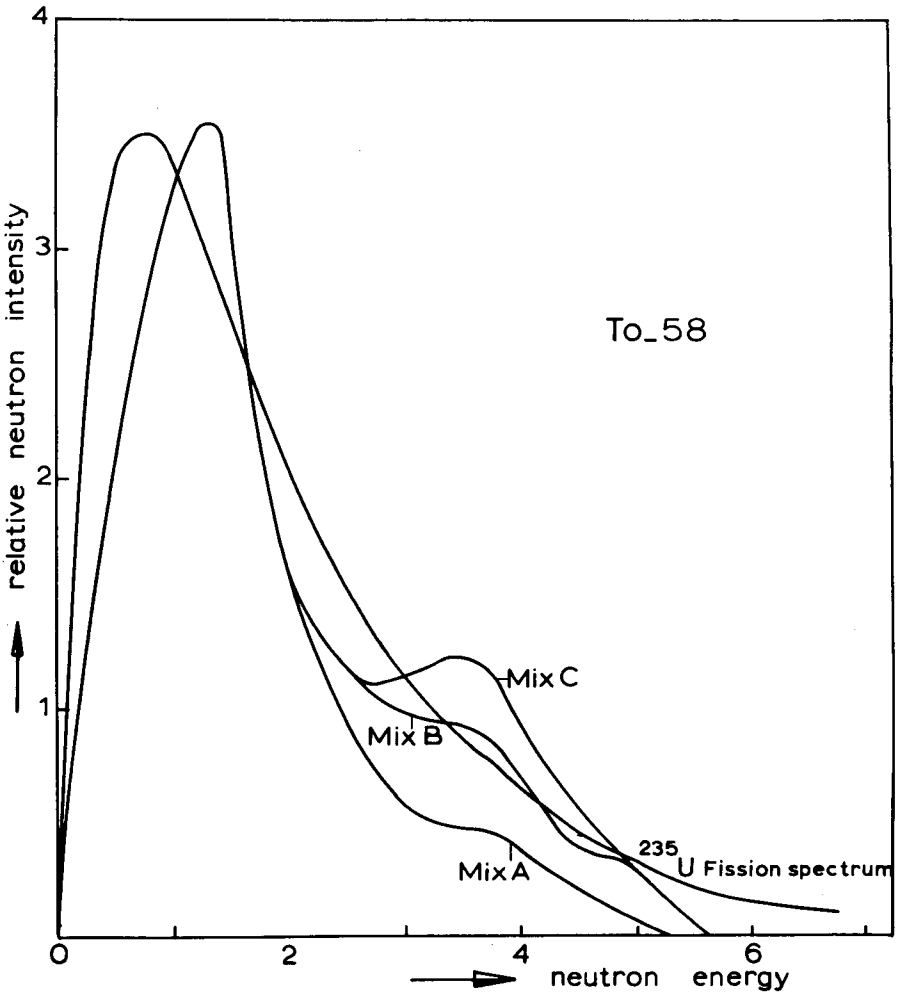

Fig. I.6 Neutron energy spectrum of a Mock-Fission source

The results obtained with the Mock-Fission neutron source used by us, show that the neutron spectrum of the source is more similar to a ^{226}RaBe spectrum (see Chapter VI).

The $^{9}Be(\gamma,n)$ neutron source: $^{124}SbBe$.

The neutron spectrum of an antimony-beryllium photo neutron source is in first approximation mono-energetic.

The neutrons of such a source have often been used to measure absolute neutron activation cross sections in the keV range (Ry 66). However, the neutron energy of such a source depends upon the dimensions and construction of the source. Essentially the scattering of the γ-rays and the single and multiple scattering of the accompanying neutrons inside the source will contribute to a low-energy tail of the primary mono-energetic neutron spectrum.

For the $^{9}Be(\gamma,n)$ reaction process the energy of the γ-ray has to be higher than the Q-value of the reaction. This Q-value has been calculated and is taken to be 1665.1 ± 0.6 keV.

The decay scheme of ^{124}Sb is known accurately. The principal γ-ray which can cause emission of neutrons has an energy of 1691.02 ± 0.03 keV. This is an average value, calculated from the ^{124}Sb γ-spectra measured by Auer (Au 69), Meyers (Me 69) and Ryves (Ry 67). From the Q-value and the γ-ray energy the initial energy of the $^{9}Be(\gamma,n)$ photo-neutrons has been calculated as 23.0 ± 1.0 keV.

For certain neutron experiments we have to make corrections for the neutron emission due to the 2090 keV γ-ray of ^{124}Sb. The energy of this neutron group is approximately 380 keV and the abundance approximately five percent (Sc 60; La 70).

To calculate the average energy of the primary neutron group, it is necessary to account for the scattering of γ-rays and of neutrons inside the source. Different calculations of the detailed energy spectrum have been published for spherical antimony-sources surrounded by spherical shells of beryllium (Be 66; Be 69; Ry 66; To 63). These Monte-Carlo calculations show that the average energy of the primary neutron group decreases as the beryllium shell thickness

increases. Because the ^{124}SbBe sources used by us contain a mixture of antimony and beryllium, it is hard to calculate the average neutron energy.

So far Lalovic (La 70) has determined the neutron spectrum of a ^{124}SbBe(Al) source of the same type we used. The average neutron energy of this source was about 1.6 keV lower than the primary energy of 26.0 keV, which is rather high.

At 23 keV the neutron scattering cross section of beryllium is high (6 barn). This means that in the ^{124}SbBe mixture a large number of neutrons will undergo elastic scattering and lose about 22 percent of their primary energy. The casing around the antimony-beryllium mixture will also have an effect on the average neutron energy. Our first ^{124}SbBe neutron source was contained in an aluminium casing of 2 mm thickness: ^{124}SbBe(Al). The scattering cross section of aluminium is about 5 b. The number of neutrons (23 keV) scattered by the aluminium casing is low and the neutron energy will not change much for this reason. The average neutron energy of the ^{124}SbBe(Al) source was estimated to be 22.0 ± 1.0 keV.

However, the second ^{124}SbBe source had a titanium casing of 2 mm thickness: ^{124}SbBe(Ti). For 23.0 keV neutrons the total neutron cross section of titanium is about 70 b. This means that the titanium casing will have a very large effect on the primary neutron spectrum, which is also seen in a very high anisotropy factor of 1.105 (Table I.1). The average neutron energy of the ^{124}SbBe(Ti) source was estimated to be 21.0 ± 1.0 keV.

The ^{124}SbBe neutron sources were used to check our renormalized neutron capture cross section curves for gold and indium, to perform transmission experiments with the ^{10}B sphere in relation to the theoretical equations of Bethe (Be 56) and to determine an efficiency curve for the electrical track counter for the neutron fission experiments

with plutonium (see Chapter III, V and VI).

The ^{252}Cf neutron source.

The construction and other characteristics of the ^{252}Cf source manufactured by an Euratom group at our laboratory has been described in detail by Kooi (Ko 67).

The Cf-mixture contained: 50 percent ^{252}Cf; 5.4 percent ^{251}Cf; 16.5 percent ^{250}Cf and 28 percent ^{249}Cf in july and august 1965.

The decay of the neutron emission was followed for several years by Mijnheer (Mij 70). The half-life for this source was found to be 2.665 ± 0.018 year.

The neutron spectrum shape of the ^{252}Cf source can be represented by the semi-empirical expression of Watt (Wa 52):

$$N(E) \sim \exp(-0.88E) \sin h\sqrt{2.0E},$$

in which N(E) is the probability of emission of a fission neutron with energy E.

An alternative expression, which gives approximately the same result, is:

$$N(E) \sim \sqrt{E} \exp(-E/T) \qquad I.1$$

This is a Maxwellian distribution for the neutron spectrum, but it is not based on a simple theoretical model. The constant T is a single parameter, called the Maxwellian "temperature". It has, however, the dimension of an energy.

The value T can be derived from neutron spectrum measurements and a number of such values are summarized in Table I.6.

From this table it can be seen that there is a rather wide spread in the data. It is easy to understand that different T-values will give noticeably different results in the calculation of any theoretical activation cross section.

Table I.6 ^{252}Cf spectrum measurements.

T (Maxwellian temperature, MeV)	Reference
1.37 ± 0.03	Bo 61
1.52	* Cl 69
1.39 ± 0.04	Co 65
1.39 ± 0.04	Gr 69
1.565	Me 67
1.40	* Mo 69
1.42 ± 0.05 }	Sm 57
1.57 ± 0.05	

weighted average value 1.39 ± 0.03

* these T-values were calculated from the published ^{252}Cf neutron spectrum.

The average T-value of 1.39 ± 0.03 was used to calculate the theoretical neutron activation cross sections and neutron fission cross sections. These results were compared with the measured average cross section values. Both results are discussed in Chapter VI.

The ^{252}Cf neutron fission spectrum was used mainly to obtain the best $^{197}Au(n,2n)^{196g+m}Au$ cross section curve and to test the $^{115}In(n,n')^{115m}In$ measurements.

The $^{241}AmLi$ neutron source.

Our $^{241}AmLi$ neutron source consists of an intimate mixture of Li and $^{241}AmO_2$. The maximum neutron energy is 1.5 MeV (Ar 68).

The neutron spectrum has been calculated by Hess (He 59), and is shown in figure I.7, together with different measurements of $^{241}AmLi$ neutron spectra and $^{210}PoLi$ spectra.

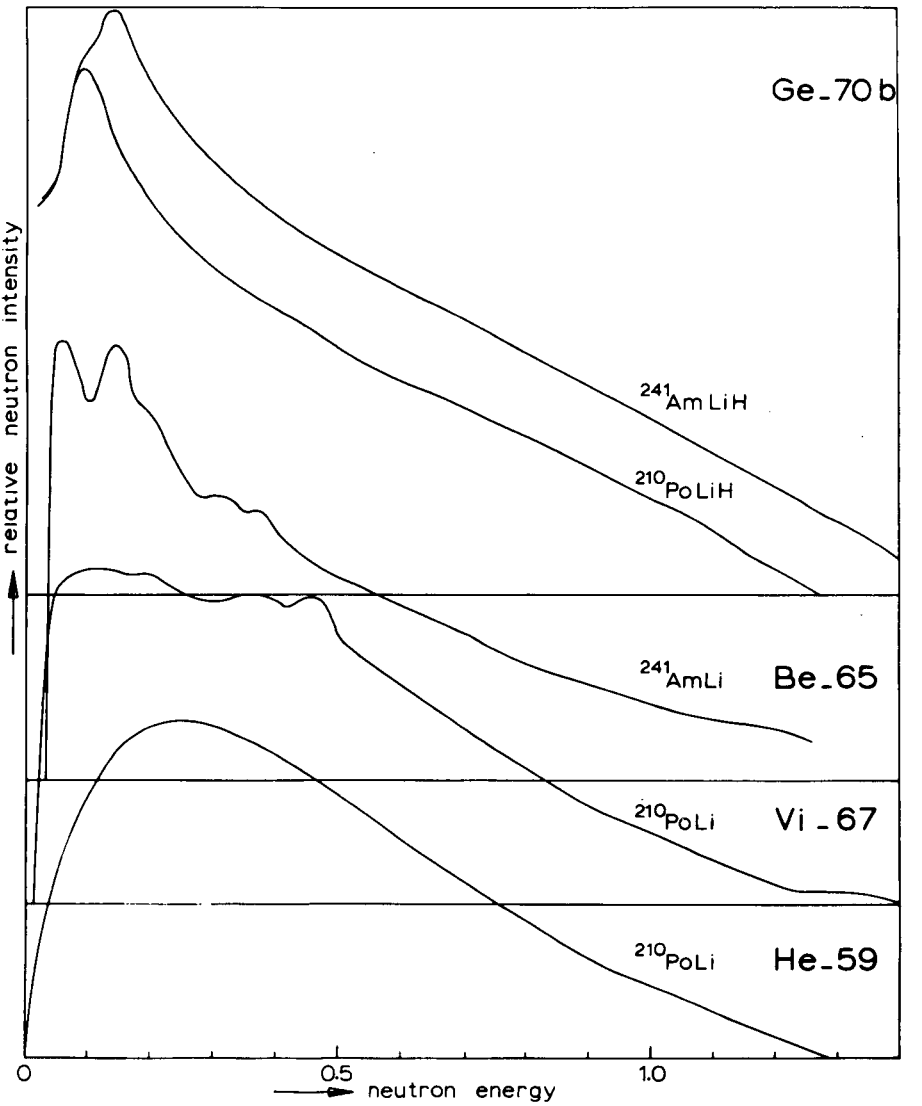

Fig. I.7 Neutron energy spectra of ^{210}PoLi and ^{241}AmLi sources

The ^{241}AmLi spectra can be compared with ^{210}PoLi spectra, because ^{241}Am and ^{210}Po alphas have about equal energies. The maximum neutron energy for a ^{210}PoLi spectrum is about 1.4 MeV (Ar 68).

From figure I.7 it can be seen that there is a wide discrepancy between the different spectra, and a large deviation from the theoretical spectrum of Hess (He 59).

The neutron spectrum of Hess was calculated under the assumption of uniform mixing of alpha emitter and lithium reaction material.
Our source, however, consists of $^{241}AmO_2$ particles. Scattering of the emitted alphas inside the $^{241}AmO_2$ particles will give lower energetic alphas to react with the surrounding Li. The neutron spectrum will be softer than the calculated spectrum.

In addition to the mixing problem, neutron scattering inside the source will cause softening of the neutron spectrum too.

The spectrum of Geiger (Ge 70b) was simulated by accelerator produced alpha particles.

As will be shown in Chapter VI, the ^{241}AmLi neutron spectrum as measured by Bennett (Be 65) is likely to be correct.

The ^{241}AmAl neutron source.

The maximum neutron energy of this source is 2.5 MeV (Table I.3). The source consists of a homogeneous mixture of Al and $^{241}AmO_2$.

As far as we know nobody has ever published a ^{241}AmAl neutron spectrum. The neutron spectrum, however, can be calculated in the way Hess did.

As in the case of the ^{241}AmLi source, the mixing problem and the neutron scattering inside the source will always soften the calculated spectrum.

The measured results will be shown in Chapter VI.

CHAPTER II

THEORETICAL ASPECTS OF NEUTRON ACTIVATION

For many purposes nuclear reactions producing radioactive isotopes are attractive for the measurement of neutrons, because of the precision with which radioactivity can be measured. The radioactivity can be detected with common β- or γ-counters.

In its simplest form the result of the interaction process of neutrons with nuclei may be written:

$$A = N\phi\sigma(1 - e^{-\lambda t}) \qquad \text{II.1}$$

in which A is the radioactivity after an irradiation time t, N the number of target atoms, ϕ the neutron flux density, σ the reaction cross section and λ the decay constant for the radioactive isotope.

In the case of fissile material, in which the fission products are captured in plastic foils, equation II.1 becomes:

$$N_f = N\phi\sigma t \qquad \text{II.2}$$

in which N_f is the total number of fission products in the plastic foil, corrected to correspond to one hundred percent detection efficiency.

Equation II.1 and II.2 can also be rewritten:

$$B = \frac{A}{N(1 - e^{-\lambda t})} \qquad \text{II.3}$$

and:

$$B = \frac{N_f}{Nt} \qquad \text{II.4}$$

in which $B = \phi\sigma$, assuming monoenergetic neutrons.

In case the neutrons have different energies:

$$B = \int_0^\infty \phi(E)\ \sigma(E)\ dE \qquad \text{II.5}$$

The calculation of the fraction of neutrons below 1.5 MeV.

Expression II.5 can be written in another form:

$$B = \int_0^\infty \phi(E)\ dE \ . \ \frac{\int_0^\infty \phi(E)\ \sigma(E)\ dE}{\int_0^\infty \phi(E)\ dE}$$

in which $\int_0^\infty \phi(E)\ dE$ is the total neutron flux density.

It is evident that the ratio $\dfrac{\int_0^\infty \phi(E)\ \sigma(E)\ dE}{\int_0^\infty \phi(E)\ dE}$

is a characteristic quantity for a neutron field. It is called the average reaction cross section $\langle\sigma\rangle_{exp}$.

$$\langle\sigma\rangle_{exp} = \frac{\int_0^\infty \phi(E)\ \sigma(E)\ dE}{\int_0^\infty \phi(E)\ dE} \qquad \text{II.6}$$

Experimentally, expression II.6 can be used to estimate the shape of a neutron spectrum if $\langle\sigma\rangle_{exp}$ values are measured for different detectors, and if $\sigma(E)$ curves are available for the different reactions involved.

In the case of the threshold detectors $^{115}In(n,n')^{115m}In$, $U(n,f)$, $^{237}Np(n,f)$ and $^{197}Au(n,2n)^{196g+m}Au$ it is possible to calculate the average reaction cross section above the threshold energy from the neutron spectrum and reaction cross section curve with sufficient precision.

$$\langle\sigma\rangle_{thr} = \frac{\int_{thr}^{\infty} \phi(E)\,\sigma(E)\,dE}{\int_{thr}^{\infty} \phi(E)\,dE} = \frac{\int_{0}^{\infty} \phi(E)\,\sigma(E)\,dE}{\int_{thr}^{\infty} \phi(E)\,dE} \qquad \text{II.7}$$

Now the fraction of neutrons above the reaction threshold is given by the expression:

$$\frac{\langle\sigma\rangle_{exp}}{\langle\sigma\rangle_{thr}} \qquad \text{II.8}$$

However, we are not specially interested in the neutron intensity above the reaction threshold of an individual detector. In the case of traditional laboratory neutron sources, like the ^{241}AmBe source, the main information we wished to obtain concerned the number and average energy of the neutrons with energies below 1.5 MeV. For this purpose we write the average cross section $\langle\sigma\rangle_{exp}$ for reactions of the type In(n,γ), Au(n,γ) and Pu(n,f) as equation II.9:

$$\langle\sigma\rangle_{exp} = \frac{\int_{0}^{\infty} \phi(E)\,\sigma(E)\,dE}{\int_{0}^{\infty} \phi(E)\,dE} = \frac{\int_{0}^{1.5} \phi(E)\,\sigma(E)\,dE}{\int_{0}^{\infty} \phi(E)\,dE} + \frac{\int_{1.5}^{\infty} \phi(E)\,\sigma(E)\,dE}{\int_{0}^{\infty} \phi(E)\,dE}$$

To know the fraction of neutrons below 1.5 MeV the first term of expression II.9 is very important and can be simplified as:

$$\frac{\int_{0}^{1.5} \phi(E)\,\sigma(E)\,dE}{\int_{0}^{\infty} \phi(E)\,dE} = \langle\sigma\rangle_{<1.5} \cdot \frac{\int_{0}^{1.5} \phi(E)\,dE}{\int_{0}^{\infty} \phi(E)\,dE} \qquad \text{II.10}$$

in which $\langle\sigma\rangle_{<1.5}$ is the average reaction cross section below 1.5 MeV and

$$\frac{\int_{0}^{1.5} \phi(E)\,dE}{\int_{0}^{\infty} \phi(E)\,dE}$$

the fraction of neutrons below 1.5 MeV.

In Chapter III it will be shown that the reaction cross section values of $In(n,\gamma)$ and $Pu(n,f)$ do not vary greatly below 1.5 MeV, at least in the energy range which provides the main activation contribution. However, this is not true for $^{197}Au(n,\gamma)$.

The second term of expression II.9 is rewritten in the following way:

$$\frac{\int_{1.5}^{\infty} \phi(E)\,\sigma(E)\,dE}{\int_{0}^{\infty} \phi(E)\,dE} = \frac{\int_{1.5}^{\infty} \phi(E)\,\sigma(E)\,dE}{\int_{1.5}^{\infty} \phi(E)\,dE} \cdot \frac{\int_{1.5}^{\infty} \phi(E)\,dE}{\int_{0}^{\infty} \phi(E)\,dE}$$

in which $\dfrac{\int_{1.5}^{\infty} \phi(E)\,dE}{\int_{0}^{\infty} \phi(E)\,dE}$ is the fraction of neutrons above 1.5 MeV and $\dfrac{\int_{1.5}^{\infty} \phi(E)\,\sigma(E)\,dE}{\int_{1.5}^{\infty} \phi(E)\,dE}$ the average reaction cross section for neutrons with an energy above 1.5 MeV, the value of which can be obtained from the known shape of the neutron spectrum combined with the known reaction cross section curve.

The fraction of neutrons below 1.5 MeV becomes:

$$\frac{\int_{0}^{1.5} \phi(E)\,dE}{\int_{0}^{\infty} \phi(E)\,dE} = \frac{\langle\sigma\rangle_{exp} - \dfrac{\int_{1.5}^{\infty} \phi(E)\,\sigma(E)\,dE}{\int_{1.5}^{\infty} \phi(E)\,dE}}{\langle\sigma\rangle_{<1.5} - \dfrac{\int_{1.5}^{\infty} \phi(E)\,\sigma(E)\,dE}{\int_{1.5}^{\infty} \phi(E)\,dE}} \qquad \text{II.11}$$

Expression II.11 is convenient to use only if the neutron spectrum contains a negligible number of neutrons with energies below 150 keV (as is the case for ^{241}AmBe, ^{239}PuBe, ^{226}RaBe and ^{242}CmBe neutron sources), because below 150 keV the cross section curves for the ^{115}In(n,γ), the ^{197}Au(n,γ) and the Pu(n,f) reactions rise very rapidly with decreasing energy.

It might be thought that the ^{197}Au(n,γ) measurements, without and in particular with the ^{10}B sphere would also be useful for the determination of the fraction of neutrons below 1.5 MeV. However, the cross section curves of ^{197}Au(n,γ) rise noticeably with decreasing energy all through the energy range below 1.5 MeV and if one has no information about the neutron spectrum below 1.5 MeV, it is not possible to calculate a sufficiently accurate value of $\langle\sigma\rangle_{<1.5}$. However, in combination with the determined fraction of neutrons below 1.5 MeV, obtained for the ^{115}In(n,γ), the U(n,f) and the Pu(n,f) measurements, the ^{197}Au(n,γ)measurements with and without the ^{10}B. sphere can be used to calculate $\langle\sigma\rangle_{<1.5}$.

From the renormalized ^{197}Au(n,γ)^{198}Au cross section curves a value may be obtained for the average neutron energy below 1.5 MeV.

In Chapter VI the calculated results have been tabulated.

CHAPTER III

NEUTRON REACTION CROSS SECTION CURVES

In Chapter II it was mentioned that for a determination of the number of neutrons below 1.5 MeV very accurate reaction cross section curves are required. The best cross section curves are obtained by renormalizing most of the literature data. Frequently even absolute measurements must be corrected, because incorrect decay schemes have been used at the time of publication.

It will, however, be demonstrated that renormalization of published values yields very satisfactory cross section curves.

The capture cross section of gold: $^{197}Au(n,\gamma)^{198}Au$.

The neutron capture cross section of gold is often used as a standard in relative neutron cross section measurements. For this reason much effort has been made to obtain correct figures, but even so different capture cross section values of gold in the literature show significant discrepancies. Some cross section curves and values are based on absolute determinations, whereas other measurements have been made relative to $^{235}U(n,f)$, $^{10}B(n,\alpha)$ and $^{6}Li(n,\alpha)$.

For the calculation of the average reaction cross section value of gold above 1.5 MeV and the determination of the neutron spectrum of various sources below 1.5 MeV, it is necessary to renormalize the literature values up to at least 10 MeV.

Poenitz (Po 68) has measured the capture cross section of gold in three ways: absolute, and relative to $^{10}B(n,\alpha)$ and to $^{6}Li(n,\alpha)$ respectively, using a "best-fit" value at 30 keV. The best fit of Poenitz' observations for gold at

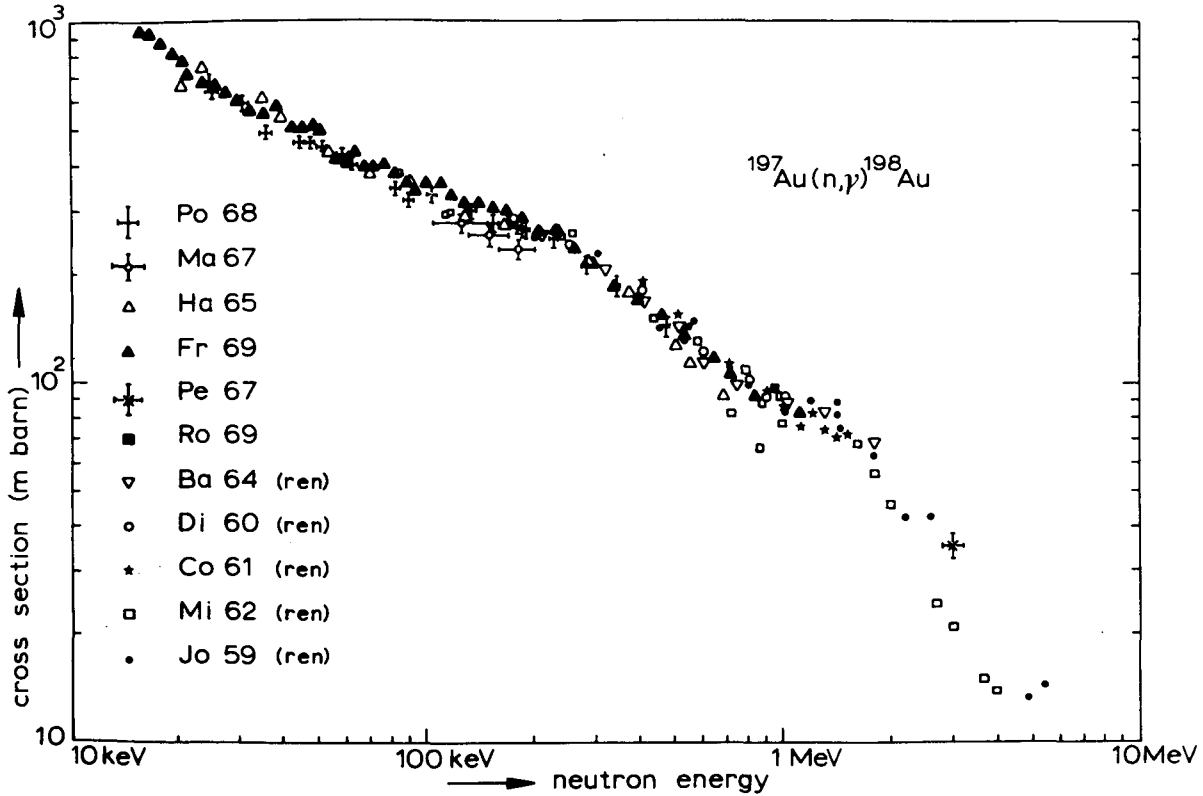

Fig. III.1 The capture cross section of gold

30 keV is 596 ± 12 mb. On the basis of this value Poenitz has determined absolute and relative cross section curves between 25 and 500 keV. The three curves are in perfect agreement below 80 keV. At higher energies there is a systematic deviation between the three curves.

On the basis of the $^{10}B(n,\alpha)$ cross section data of Gubernator (Gu 68), the values of Poenitz (above 80 keV) and of Mäcklin (Ma 67), both relative to the $^{10}B(n,\alpha)$ cross section, should be raised by about 10 percent. If this is done the absolute measurements of Harris (Ha 65) and the results of Fricke (Fr 70) agree with those of Poenitz.

The measurements relative to $^{235}U(n,f)$ of Diven (Di 60), Cox (Co 61) and Johnsrud (Jo 59) have been renormalized using the $^{235}U(n,f)$ cross section curve of Hart (Ha 69).

The renormalized capture cross section curves of gold obtained in this way have different absolute values but roughly the same shape, and it seems justified to renormalize all of them on the basis of the general shape of the curve given by Poenitz, Harris and Fricke.

The absolute measurements of Barry (Ba 64) and Miskel (Mi 62) have been renormalized in the same way.

The 3.0 MeV point of Petö (Pe 67) was measured relative to $^{31}P(n,p)$ and $^{32}S(n,p)$. This has been renormalized on the basis of $\sigma^{31}P(n,p)^{31}Si$ = 74 ± 6 mb and $\sigma^{32}S(n,p)^{32}P$ = 111 ± 10 mb at 3.0 MeV.

Our own absolutely measured $^{197}Au(n,\gamma)^{198}Au$ cross section values of 715 ± 30 mb for SbBe(Ti) neutrons (21.0 keV) and 655 ± 40 mb for SbBe(Al) neutrons (22.0 keV) agree well with the cross section curve of gold derived by the renormalization procedure described (figure III.1).

The $^{197}Au(n,2n)^{196g+m}Au$ cross section.

From the very low ^{196}Au activity the number of very fast neutrons above the reaction threshold of 8.1 MeV can be determined for the different neutron sources. However, for

such calculations a very good cross section curve is required.

In the energy range 8.1 to 20 MeV there are only two independent cross section measurements by Tewes (Te 60) from (8.2 - 15.1 MeV) and by Prestwood (Pr 61) from (12.15 - 19.75 MeV), which overlap satisfactorily. Apart from these two there are many individual cross section measurements around 14 MeV.
The values are shown in Table III.1.

Only the average values have been placed in the cross section plot (figure III.2).

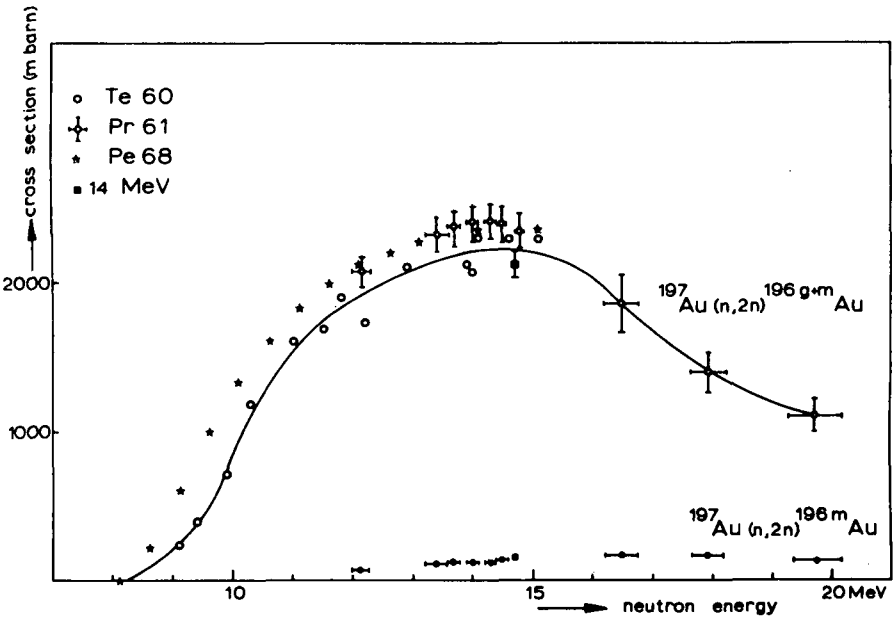

Fig. III.2 The $^{197}Au(n,2n)^{196g+m}Au$ cross section

Recently a theoretical cross section curve has been determined, using the equations of Pearlstein (Pe 68). In the interesting energy range between 8.1 and 12 MeV a serious discrepancy exists between the measured cross section curve of Tewes and the theoretical curve of Pearlstein.

Table III.1 The $^{197}Au(n,2n)^{196g+m}Au$ cross section around 14 MeV.

ref.	MeV	$\sigma^{(mb)}_{g+m}$	$\sigma^{(mb)}_{m}$	neutron monitor
Pa 53	14.7	1722 ± 465		absolute
Gr 55	14.7	1525 ± 305		absolute
As 58	14.1	2600 ± 200		absolute
Iz 60	14.7	1800 ± 500		?
Ma 65	14.8	1950 ± 175	230 ± 35	$^{27}Al(n,p)^{27}Mg$
Vo 68	14.7	2320 ± 180	148 ± 15	$^{27}Al(n,\alpha)^{24}Na$
Ha 68	14.4	1986 ± 200	151 ± 18	$^{56}Fe(n,p)^{56}Mn$ { $^{27}Al(n,\alpha)^{24}Na$
Te 60	14.3	2200 ± 220		absolute
Pr 61	14.3	2400 ± 120		absolute
average value	14.6	2120 ± 90	160 ± 10	

If the ^{252}Cf neutron spectrum (eq. I.1 with T = 1.39±0.03) is assumed to be correct, comparison between our activation measurements with such a source and the calculated activity indicates that the cross section curve published by Tewes is at least approximately correct, whereas the theoretical curve of Pearlstein is definitely too high (see for details Chapter VI).

The capture cross section of indium.

$^{115}In(n,\gamma)^{116m}In$ (54 minute activity)

To obtain a capture cross section of indium it is necessary to renormalize the curves and values in the literature in the same way as it has been done for the capture cross section of gold.

Grench (Gr 68a) has made measurements relative to $^{197}Au(n,\gamma)$. For the renormalization the gold capture cross section curves of Poenitz, Harris and Fricke have been used.

From γ-spectra measurements we determined that the

1.29 MeV γ-ray accompanies 83.7 ± 1.6 percent of the decays. In the renormalization process this value was used instead of 82 ± 3 percent as assumed by Grench.

The data of Menlove (Me 67a), Cox (Co 64) and Johnsrud (Jo 59) relative to $^{235}U(n,f)$ have been treated as mentioned in the description of the gold capture cross section curve.

The capture cross section curve obtained in this way is in good agreement with the 3.0 MeV points of Petö (Pe 67), relative to $^{31}P(n,p)$ - 74 ± 6 mb - and $^{27}Al(n,p)$ - 2.5 ± 0.2 mb - and Colditz (Co 68) relative to $^{115}In(n,n')^{115m}In$ - 360 mb -.

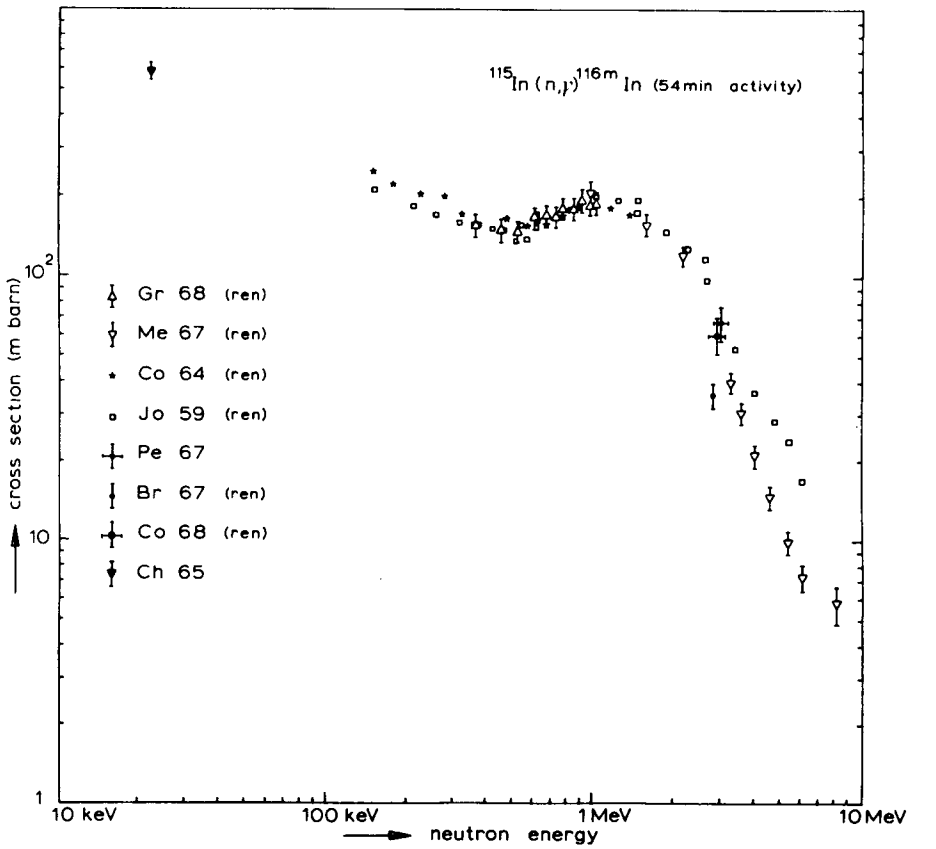

Fig. III.3 The capture cross section of indium $^{115}In(n,\gamma)^{116m}In$ (54 min. activity)

The value of Broadhead (Br 67) relative to $^{115}In(n,n')^{115m}In$ - 360 mb - is probably too low.

The renormalized indium cross section curves of Johnsrud and Menlove agree very well with each other below about 2 MeV. At higher energies, however, they start to diverge, and above 5 MeV their values differ by a factor 2 at least. For our calculations an average capture cross section curve has been used.

Capture cross section measurements below 100 keV are rare. Here the cross section curve of indium has been extrapolated through the value of 640 ± 40 mb for SbBe(Ti) neutrons (21.0 keV) and 550 ± 50 mb for SbBe(Al) neutrons (22.0 keV) measured by us (figure III.3). Our measurements at these energies are in agreement with the value determined by Chaubey (Ch 65).

The inelastic scattering cross section of indium.

$^{115}In(n,n')^{115m}In$ (4.50 hour activity)

In the cross section curve of indium (figure III.4) the measurements of Cohen (Co 48) and Martin (Ma 54) are not included, because the renormalization of those curves is very difficult and the agreement between both curves is poor.

Heertje (He 63) has determined the average cross section of indium for a $^{226}RaBe$ neutron source. Out of this result he constructed an indium cross section curve, the shape of which is in very good agreement with the later measurements of Grench (Gr 68), Menlove (Me 67b) and Butler (Bu 67).

The cross section values of Grench and Menlove relative to $^{197}Au(n,\gamma)$ and $^{235}U(n,f)$ respectively, have been renormalized as described for the $^{115}In(n,\gamma)^{116m}In$ cross section curve.

The 14 MeV result of Nagel (Na 64) is in agreement with the renormalized cross section curve.

To check this renormalized curve the average reaction cross section for the mentioned ^{252}Cf neutron spectrum

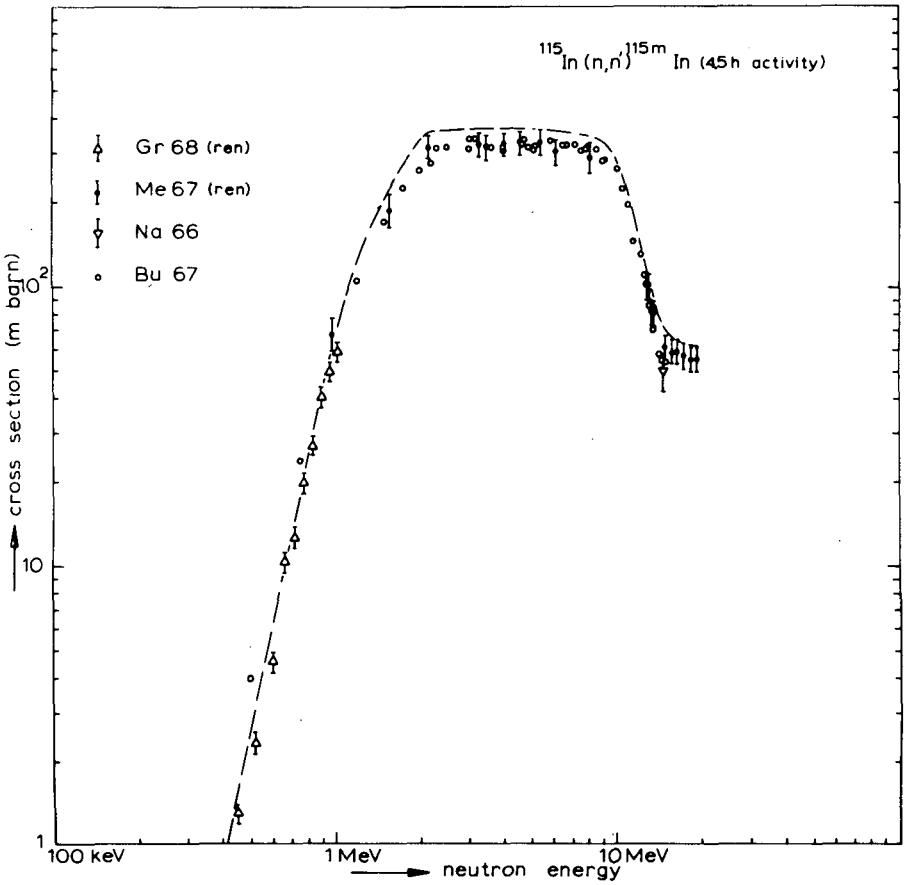

Fig. III.4 The inelastic scattering cross section of indium: $^{115}In(n,n')^{115m}In$ (4.50 hour activity)

----- proposed cross section curve (see Chapter VI)

(eq. I.1, with T = 1.39 ± 0.03) was calculated. The calculated result is in good agreement with the measured one (see Chapter VI).

The influence of the ^{10}B sphere on the $^{197}Au(n,\gamma)$ and $^{115}In(n,\gamma)$ cross section curves.

In first approximation the transmission T_a of neutrons through a ^{10}B shell of thickness N^B (the number of ^{10}B atoms per cm^2) is frequently represented by the expression:

$$T_a = e^{-\sigma_a^B N^B} \qquad \text{III.1}$$

in which σ_a^B is the absorption cross section of ^{10}B.

In this equation the elastic scattering of neutrons is neglected because it is assumed that as many neutrons are scattered into the interior of the shell as there are scattered out of it. In fact such scattering leads to an increased path length in the shell and therefore it increases the probability of absorption.

Bethe (Be 56) has shown that because of this effect the transmission T even for thin shells is more accurately given by the expression III.2

$$T = 1 - (1 - e^{-\sigma_t^B N^B}) \frac{\sigma_a^B}{\sigma_t^B} \left\{ 1 + \frac{\sigma_s^B}{\sigma_t^B}(1-P_1) + \frac{(1-P_1)(1-P_2)(\sigma_s^B)^2}{\sigma_t^B(\sigma_a^B + \sigma_s^B P_m)} \right\}$$

in which σ_t^B is the total cross section of ^{10}B and σ_s^B the elastic scattering cross section of ^{10}B ($\sigma_t^B = \sigma_s^B + \sigma_a^B$).

The values of P_1, P_2 and P_m are tabulated by Bethe and are the probabilities that a neutron will enter the detector after one, two or more elastic collisions in the shell.

Bethe's equation can be used only if the elastic scattering of neutrons does not result in an important change in energy, i.e. it is restricted to scattering from relatively heavy nuclei. In the case of ^{10}B this is not strictly valid.

The only ^{10}B shell transmission experiments have been done by Basson (Ba 62). His experimental results are in reasonable agreement with the one expected on the basis of Bethe's equation. For this reason it seems justified to use

eq. III.2 for the calculation of the effective cross section of gold and indium

The transmission values T_a and T have been calculated for different neutron energies on the basis of the total ^{10}B cross section values of Diment (Di 67) and the absorption ^{10}B cross section values of Gubernator (Gu 68).

The results are shown in Table III.2.

Table III.2 The transmission factors for a 2.2 g per cm^2 ^{10}B sphere.

neutron energy (keV)	T	T_a	neutron energy (keV)	T	T_a
10	0.418	0.452	100	0.734	0.767
20	0.558	0.585	200	0.787	0.820
30	0.589	0.625	300	0.842	0.869
40	0.622	0.659	400	0.869	0.892
50	0.655	0.690	500	0.875	0.896
60	0.686	0.718	600	0.908	0.921
70	0.705	0.737	700	0.926	0.936
80	0.715	0.747	800	0.940	0.948
90	0.730	0.762	900	0.945	0.955

At energies above 1 MeV the values of T_a and T become equal.

The effective cross section curves of gold and indium are shown in figure III.5.

To check eq. III.2 transmission experiments have been done with ^{124}SbBe neutrons (22.0 and 21.0 keV). The transmission value for ^{124}SbBe(Al) neutrons is in agreement with the calculated one, while the transmission value for SbBe(Ti) neutrons is lower than expected from formula III.2 (see Chapter VI).

This can be understood, if it is assumed that by scattering within the neutron source itself the monoenergetic

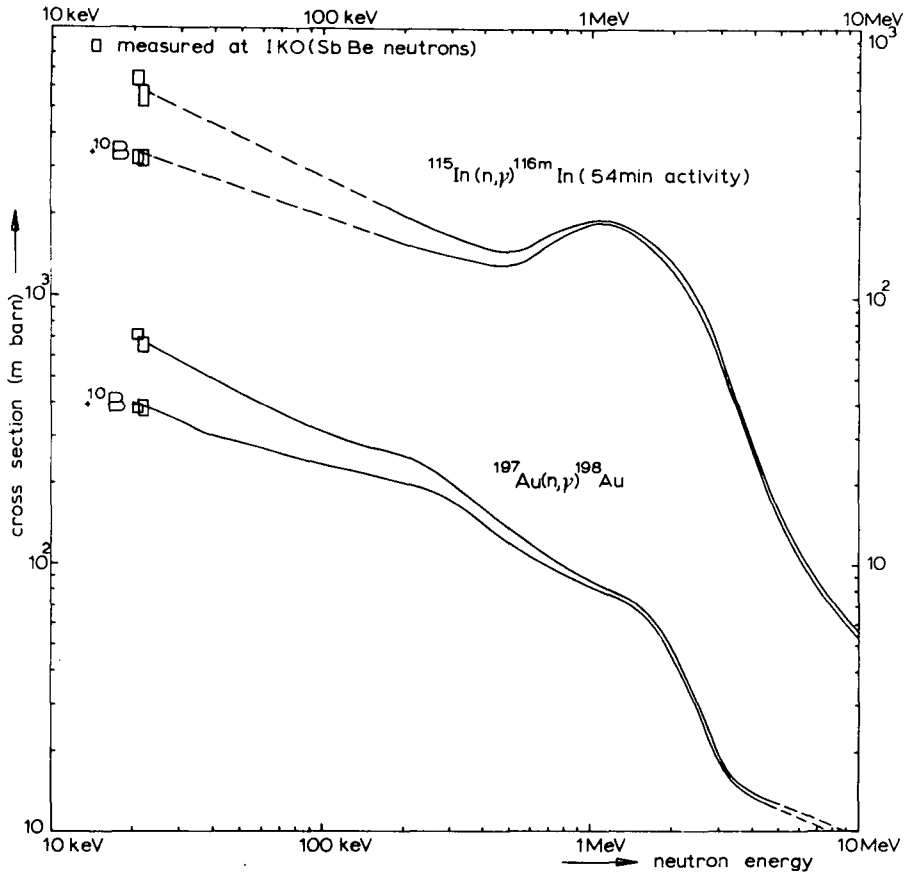

Fig. III.5 The effective cross section of $^{197}Au(n,\gamma)^{198}Au$ and of $^{115}In(n,\gamma)^{116m}In$ for a 2.2 g per cm^2 ^{10}B sphere.

neutron spectrum is extended to energies lower than 21.0 keV. The low energy tail is more strongly absorbed by the ^{10}B sphere than are neutrons of the original energy. The transmission value will be lower than the one corresponding to the average neutron energy (see Chapter I).

The (n,f) cross section curves of ^{237}Np, natural U and Pu.

For the construction of the (n,f) cross section curves shown in figure III.6, the revised data of Hart (Ha 69) have been used.

The Pu fissile material contained 98.358 percent ^{239}Pu; 1.613 percent ^{240}Pu; 0.029 percent ^{241}Pu and < 0.0005 percent ^{242}Pu.

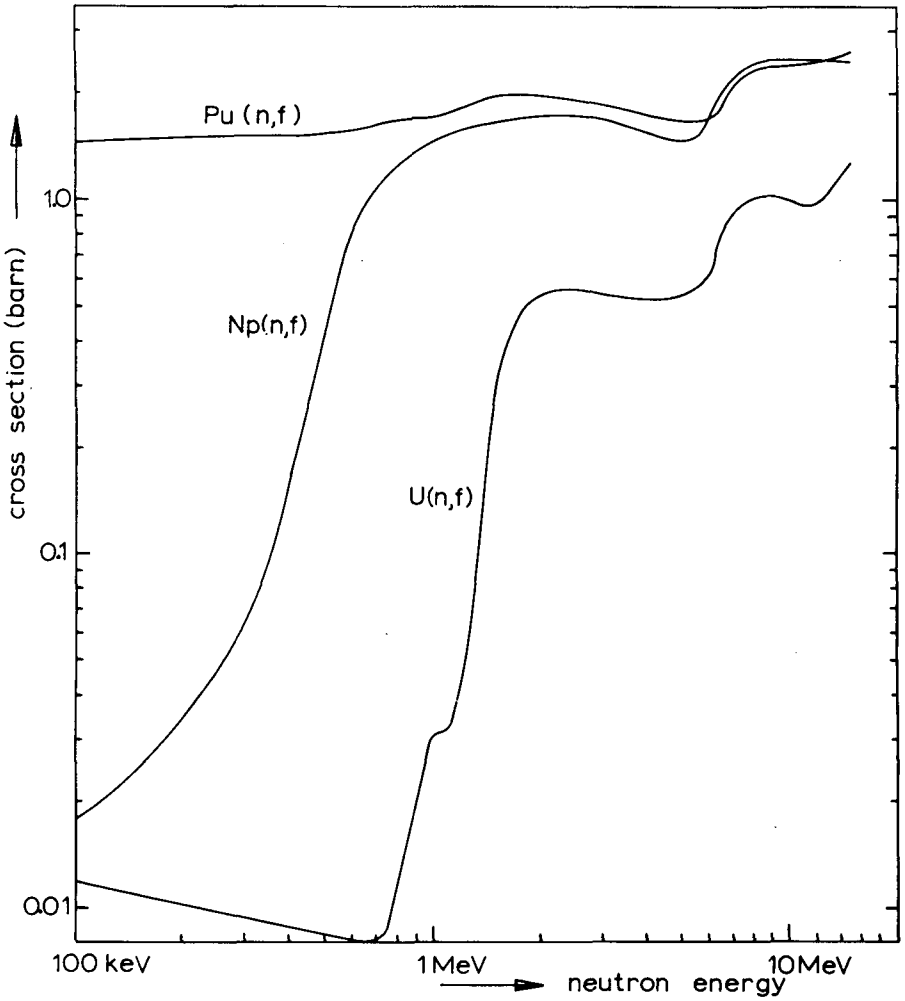

Fig. III.6 The (n,f) cross section curves of ^{237}Np, natural U and Pu.

Table III.3 The renormalized cross sections of the different neutron detectors

neutron energy	cross sections (mb)						
keV	$^{197}Au(n,\gamma)$	$^{197}Au(n,2n)$	$^{115}In(n,\gamma)$	$^{115}In(n,n')$	$^{237}Np(n,f)$	U(n,f)	Pu(n,f)
21 - SbBe(Ti)	715 ± 30*		640 ± 40*				1700 ± 200*
22 - SbBe(Al)	655 ± 40*		550 ± 50*				
30	600 ± 5%		(500)		11 ± 10%	16 ± 10%	1585 ± 10%
60	430		(360)		13	13	1450
100	330		280 ± 10%		18	12	1450
200	260		200		35	10	1500
400	170		154		† 169	9	1520
500	145		148	2.0 ± 10%	2 ± 10% 420	8	1540
600	120		160	5.2	6 690	8	1575
800	100		182	24	27 1270	12	1690
1000	90		194	66	75 1470	31	1715
1200	85		193	120	135 1560	48	1805
1600	70		165	220	250 1650	365	1980
2000	50		135	310	350 1700	540	1985
2500	35		98	320	360 1730	560	1935
3000	21		64	320	360 1690	540	1865
4000	14		29	325	365 1550	525	1750
6000			11.3	320	360 1730	615	1690
8000			7.4	290	330 2380	1005	2300
9000		200 ± 10%	6.4	270	305 2440	1025	2395
10.000		850	5.8	230	260 2450	1000	2395
11.000		1550	5.8	200	220 2450	980	2400
12.000		1900	5.8	130	147 2440	970	2455
13.000		2100	5.8	100	110 2440	1050	2500
14.000		2200	5.8	70	79 2440	1160	2575

* measured at I.K.O.

† proposed cross section data (see Chapter VI)

CHAPTER IV

CALIBRATION OF THE NEUTRON ACTIVATION DETECTORS

The gold and indium activities were measured in a 3 x 3 inch NaI(Tl) well-type crystal. The instrument was mounted inside a special shielding in such a way that it can be used as a low-level gamma counter. Its efficiency in terms of a desintegration rate per count has been determined by De Ruyter (Ru 68) at various energies using 10 ml solutions.

Because of the very low activities present after the neutron irradiation of gold and indium foils, we used instead gold and indium spheres of 1 cm diameter.

Activity corrections due to neutron flux depression and neutron scattering inside the sphere are negligible (Be 56).

The gold and indium spheres were counted at the bottom of the well. The measured activities were about 1 - 1000 counts per minute (dependent on the neutron source strength) above a background of about 40 counts per minute.

Gold.

The ^{198}Au isotope, formed by the reaction $^{197}Au(n,\gamma)^{198}Au$ has a single gamma-ray of 412 keV. The gamma-ray is emitted in 96.0 percent of the decays.

The gold activity was measured by counting over the gamma-energy range 292 - 518 keV.

After each gold irradiation the decay was followed for several days. It was found that a small fraction of the measured activity was due to the formation of $^{196g+m}Au$, resulting from the reaction $^{197}Au(n,2n)^{196g+m}Au$. To determine

the exact $^{198}Au/^{196g+m}Au$ activity ratio for each neutron source, long irradiations were performed and the decay was followed for at least 40 to 50 days. From these measurements the $^{198}Au/^{196g+m}Au$ activity ratio could be determined per minute irradiation time and per gram gold, assuming a half-life of 3880 minutes for ^{198}Au and 8900 minutes for $^{196g+m}Au$.

To calculate the absolute gold activities, using the efficiency curve measured by De Ruyter, we have to correct for the self-absorption of the gamma-rays inside the gold sphere. For this reason two long gold irradiations were performed with the $^{239}PuBe$ source. For both gold spheres the activities were followed for about a week. Then the gold spheres were dissolved in aqua regia and the solutions were diluted to 500 ml to avoid self-absorption values different from them in dilute solutions for which the instrument has been calibrated. For each gold solution four samples were taken of 2 x 10 ml and 2 x 5 ml. The last two samples were diluted again to 10 ml distilled water to establish that the self-absorption difference in the solution is really negligible. All four samples of 10 ml were counted in the in-well position of the 3 x 3 inch NaI(Tl) crystal. The activities were followed for about two weeks. At that time most of the 10 ml solutions showed the beginning of a precipitate. Therefore the radioactivity was no longer homogeneously distributed. However, activity measurements in a two week period are too short to analyse the complex decay curve of a mixture of ^{198}Au and $^{196g+m}Au$.

To make corrections for the $^{196g+m}Au$ activity in the 10 ml solutions, two other gold spheres surrounded by Cd-shields were irradiated with fast neutrons (deuterons of 25 MeV on a Be target in the IKO synchrocyclotron). A Ge(Li) gamma-ray spectrum did not show any ^{198}Au activity. To exclude any small ^{198}Au activity we waited one month before both gold spheres were measured several times in the in-well position and handled in the same way as described above.

Three gamma-rays with energies 333 keV, 356 keV and 426 keV contribute to the $^{196g+m}$Au activity in the energy range 292 - 518 keV. Its relative intensities have been accurately measured by Jansen (Ja 67). In this way the correction factors for self-absorption were determined both for ^{198}Au and $^{196g+m}$Au.

Indium.

Fast neutron irradiation of the indium spheres shows two activities, which belong to the 54.13 minute activity of ^{116m}In and the 4.50 hour activity of ^{115m}In.

The ^{115m}In decays by an isomeric transition to the ground state of ^{115}In. The energy of the gamma-ray is 335 keV and the gamma-ray accompanies 50.0 percent of the decays.

The ^{116m}In decays to different excited states of ^{116}Sn. The energy of the strongest gamma-ray is 1293 keV. Because the gamma-ray spectrum is complex, it is hard to calibrate ^{116m}In on one special gamma-ray with the low-level gamma counter.

The calibration procedure of both indium isotopes was similar to the one described for gold. However, instead of using a single channel system, as was done for the gold calibration, the well-type crystal was coupled to a 400 channel analyser (energy range 0 - 2500 keV). The analyser was set in such a way that the gamma spectrum of the isotope mixture was typed out at one hour intervals. Every measurement lasted at least 9 hours.

The ^{116m}In activity was measured by summing all channels in the energy range 700 - 2430 keV. The sum spectrum of each one hour period was plotted to check the half-life of ^{116m}In. The correct value was obtained.

The lower limit was located at 700 keV in order to avoid any activity due to pile up of the 335 keV gamma-ray of ^{115m}In.

The sensitivity in the integrated energy range be-

tween 700 and 2430 keV was determined with the help of a Ge(Li) crystal calibrated for the determination of absolute activities. A weighed amount of a very active solution of ^{116m}In was diluted to 10 ml and measured in the NaI(Tl) well-type crystal. Another aliquot of the same solution was dried and measured on the calibrated Ge(Li) crystal. By the latter measurement the absolute intensity of the 1293 keV gamma-ray was determined. The whole procedure was repeated several times to obtain good statistics. The decay scheme of ^{116m}In is at present well known. Two gamma-rays of 1293 keV and 2110 keV decay directly to the ground state of ^{116}Sn. Different spectrum measurements showed that the absolute gamma-intensity ratio of those gamma-rays was 5.14 ± 0.10. This means that for the strong 1293 keV gamma-ray the gamma-abundancy is 83.7 ± 1.6 percent.

The data obtained in the first five hours of each decay curve were used to calculate the ^{116m}In activity at the end of each neutron irradiation. Only the last hours of each decay curve were suitable for determining the ^{115m}In activity because the ^{116m}In activity disturbs the ^{115m}In spectrum.

The indium activities were so low, that no correction was needed for pile up for the in-well position of the NaI(Tl) crystal.

CHAPTER V

USE AND CALIBRATION OF FISSION DETECTORS

It has been known for several years that fission fragments can be detected with different kinds of electrically insulating solids. In those materials fission fragments with kinetic energies in the MeV range produce narrow tracks of radiation damage, which may be observed directly with an electron microscope.

In many materials such tracks are known to be preferentially attacked by suitable chemical reagents. In these materials they can be enlarged by prolonged chemical etching in such a way that they become visible under an ordinary optical microscope. The number of tracks counted under the microscope is then a measure of the number of fission fragments, which have penetrated into the insulating solid.

In our work we have made use of this simple method to detect neutrons. Interaction of neutrons of suitable energy with plutonium, neptunium or uranium causes fission, the fragments of which are registered in an electrically insulating solid, called Makrofol KG. (This is the Bayer A.G. trade name for polycarbonate foil.)

The fissile material was electroplated on 1 mm thick nickel disks of 19 mm diameter. The diameter of the fissile material on the nickel disk was 12 mm. The nickel disks held about 0.1 mg of fissile material. Such very thin layers were used to avoid absorption of the fission fragments within the fissile material as far as possible.

The Makrofol K.G. plastic was 12μm thick and was placed directly against the fissile material to avoid absorption of fission fragments in air.

As a standard etchant we used NaOH of 6 N concentration.

For all electrically insulating solids the etching condition is rather critical. In the case of Makrofol K.G. bubble formation can occur at temperatures above 70°C. However, at room temperature long etching times are required. For this reason we have developed our own etching technique. The fission tracks were counted in two manners: by means of an optical microscope and by means of a specially constructed electrical track counter.

The etching conditions.

For a reproducable etching method the temperature inside the etchant should be held below 70°C and within a certain temperature range.

We therefore constructed a special vessel with double walls between which methanol vapor is refluxed. The temperature of the methanol vapor is 65°C. The etchant was heated by the methanol vapor, after which the Makrofol K.G. foils were etched for a suitable time. The temperature inside the etchant remained at (64 + 1)°C throughout the etching time.

Figure V.1 shows the variation of the number of fission tracks counted under the optical microscope with the duration of the etching. These tracks were made by fission fragments from a thin source of ^{252}Cf, electroplated on to a nickel disk. The fission fragments pass through the Makrofol K.G. foil at different angles to its surface. It is to be expected that the number of tracks becomes constant when the etching time exceeds a certain value.

Cross (Cr 69) stated that this is not true for a thick layer of fissile material. In this case the number of tracks does not become constant at long etching times.

To avoid this complication the Makrofol K.G. foils were always etched in the same way for a constant time (one hour), which was selected to suit the characteristics of the electrical track counter.

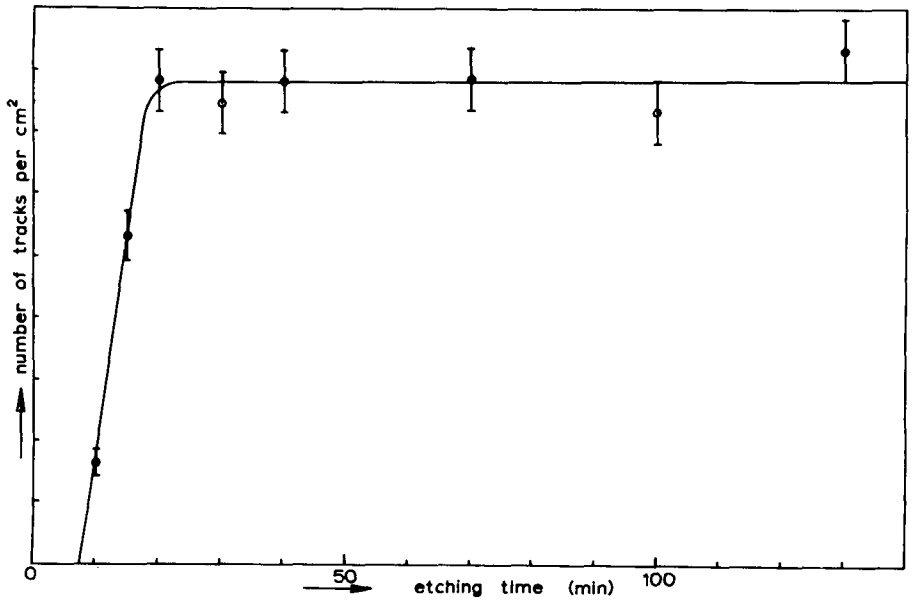

Fig. V.1 The number of tracks counted under the optical microscope as a function of the etching time.

The optical microscope.

The Makrofol K.G. foils, etched for one hour in a 6 N NaOH solution were counted under the optical microscope (magnitude 250 x), Because in our experiments the plastic foils are put directly on top of the fissile material, the fission fragments enter at all angles between 0 and 90 degrees. Under these circumstances the detection efficiency is less than 100 percent. An electroplated ^{252}Cf source, calibrated by means of its α-emission in a low geometry counter, was used to measure the detection efficiency. The efficiency was about 70 percent. This is easily understood when it is realised that etching removes a surface layer of about one μm thickness from the plastic foil. Apart from this Lark (La 69) observed that no fission fragments will be

detected in plastic foils, the entering angle of which is smaller than 10^{o}. He also noticed that no tracks were seen in foils of 2 μm thickness or less. From this he concluded that fission particles are registered only if their tracks penetrate into the plastic to a depth of at least 2 or 3 μm.

For large track densities, 10^{3} - 10^{4} tracks per cm^{2}, the counting under the optical microscope is very reproducible even if counting is performed by different persons. However, in the case of small track densities, well below 10^{3} tracks per cm^{2}, deviations up to 30 percent were found to occur in counting the same plastic foil. This could be accounted for by the irregularities in the Makrofol K.G. plastic, which in many cases cannot with certainty be distinguished from real tracks.

In our measurements the optical microscope was used only to check the etching by measuring the track diameter. For routine purposes an electrical track counter was constructed.

The electrical track counter (ETC).

After the chemical etching the tracks are seen as small holes in the plastic foil, which, in the case of thin foils penetrate from one side to the other. The holes in the plastic foil can be counted electrically by placing it as an isolating layer between two high voltage electrodes of a spark gap. At the location of a hole, isolation is lacking and a spark occurs. The sparks will enlarge the holes to a size visible to the unaided eye. By connecting the electrical system to a scaler, the number of sparks can easily be counted.

Lark (La 68) has made use of a similar principle. He replaced the optical magnification system of a scanning microscope by a pen electrode. The scanning table serves both as the grounded plane electrode and to hold the plastic foil. In this technique one still has to scan the plastic foil

which requires much time and a complicated construction.

A simpler method was introduced by Cross (Cr 69), who placed the isolating plastic foil between two plane electrodes, after which the holes in the foil could be counted in a few seconds.

On the basis of this development an electrical track counter was constructed in our laboratory.

The grounded plane electrode was made of a thin layer of nickel, electroplated on copper. The opposite electrode consists of a thin layer of aluminium, evaporated on a Mylar backing of 25 μm thickness (Westfälische Metall Industrie KG). The electrical connections for the whole system are shown in figure V.2.

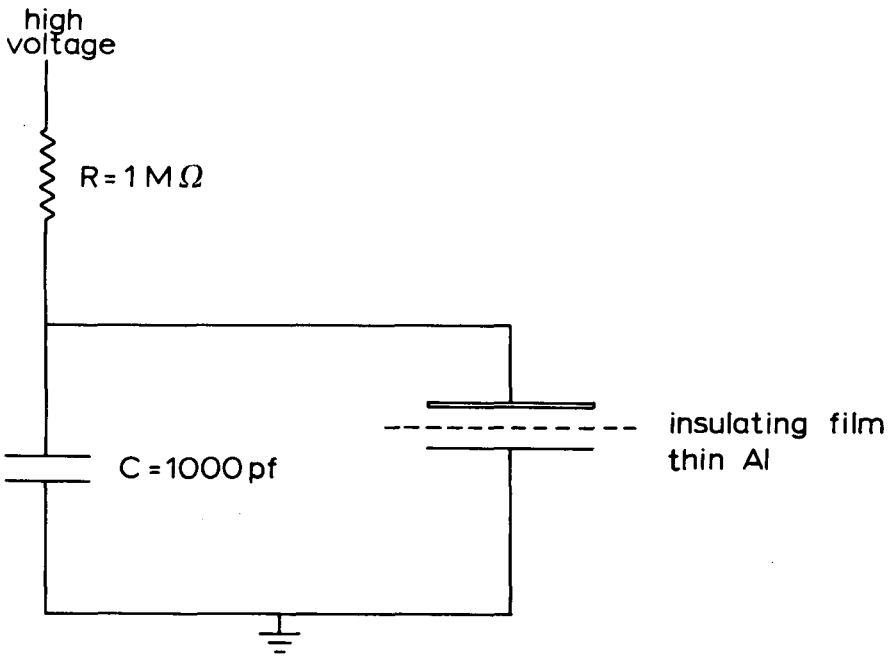

Fig. V.2 The electrical connections of the ETC.

When a high voltage is applied, a spark will pass through one of the holes in the plastic foil and produces a much larger hole in the thin aluminium electrode. The spark is quenched by the capacitor. After the capacitor has been recharged, a second spark cannot pass through the same hole, because the path to the edge of the hole in the aluminium layer has become too long. The next spark therefore passes through another hole. In this way the discharge jumps from one hole to another until it has passed through all the holes. The discharge then stops.

For this procedure it is necessary to make the voltage and capacitance match the thickness of the aluminium layer and the distance between the two plane electrodes. The aluminium electrode now presents an imprint of the plastic foil. The number of holes in the aluminium electrode can be counted by the unaided eye and can be compared with the number read from the scaler. The agreement was satisfactory and demonstrated that the electrical track counter works correctly. It can be used as a simple instrument to measure neutron doses with reasonable speed and accuracy.

It was found that the diameter of the holes in the aluminium electrode and the number of sparks counted is a function of the high voltage applied to the plastic foil (figure V.3).

The graph shows that the characteristics of the electrical track counter are similar to those of a normal GM-counter. Above 650 V the spark has enough energy to start through the same hole a second time. The length of the plateau depends on the magnitude of the capacitor discharge. For every 100 V the number of sparks rises by 4 percent.

Before counting the holes a voltage of 1150 V is applied. The large sparks produce vertical holes in the insulating foil of constant diameter. A second sheet of aluminized Mylar is then used to count these holes at 560 V.

When we counted the same plastic foil several times at 560 V it was noticed that the reproducibility was within

1 percent for numbers of sparks below about 500 per cm^2. At higher densities the reproducibility becomes worse and deviations of up to maximum 10 percent are normal for duplicate measurements.

To know the background of Makrofol K.G., different foils were counted with the ETC. No sparks occured through the unetched foils. For etched foils the background was a function of the etching time.

The results are shown in Table V.1.

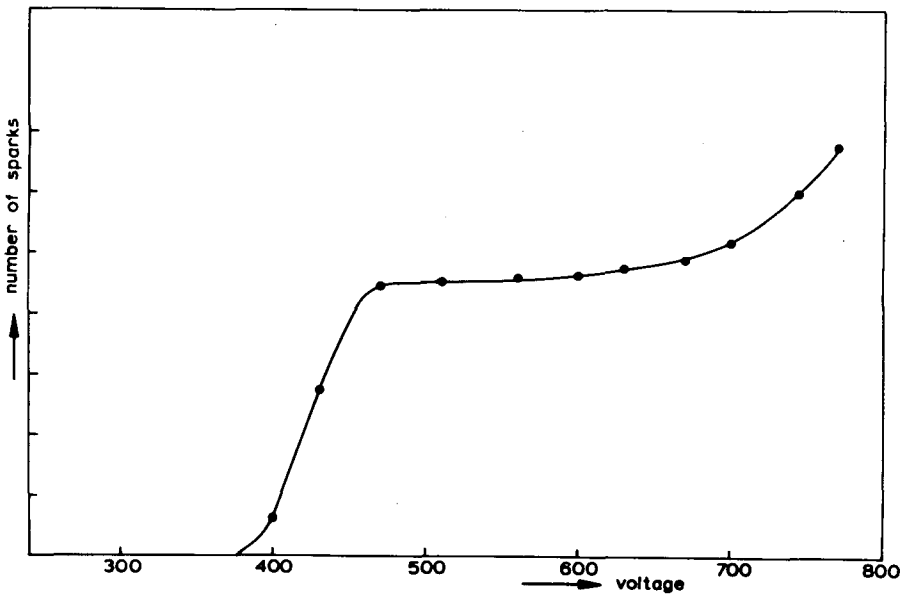

Fig. V.3 The number of sparks counted with the ETC as a function of the high voltage.

Table V.1 The electrical track counter background per cm^2 for 12 μm Makrofol K.G. foils.

etching time (min)	number of sparks per cm^2 (ETC)
0	0
30	0
60	0.6
90	3.5
120	> 20

This table is easily understood. For larger etching times more material is removed from the foil by the etchant. As the foil becomes thinner, the isolation between the two plane electrodes becomes worse, more sparks will occur.

As was shown in figure V.1 for Makrofol K.G. foils an etching time of 30 minutes is about the minimum. To be on the safe side we selected for our experiment an etching time of 60 minutes.

There is also a second argument for this selection. The efficiency of the ETC depends on the etching time. This relation is seen in figure V.4.

Etching times longer than 60 minutes do not contribute much to the ETC efficiency.

The ETC efficiency.

For the fissile materials plutonium, neptunium and uranium over-all track counting efficiencies as a means for fission registration were determined for an etching time of 60 minutes.

The amount of fissile material of each sample was calculated from activity measurements with a calibrated α-counter. The samples we used have the following isotopic composition:

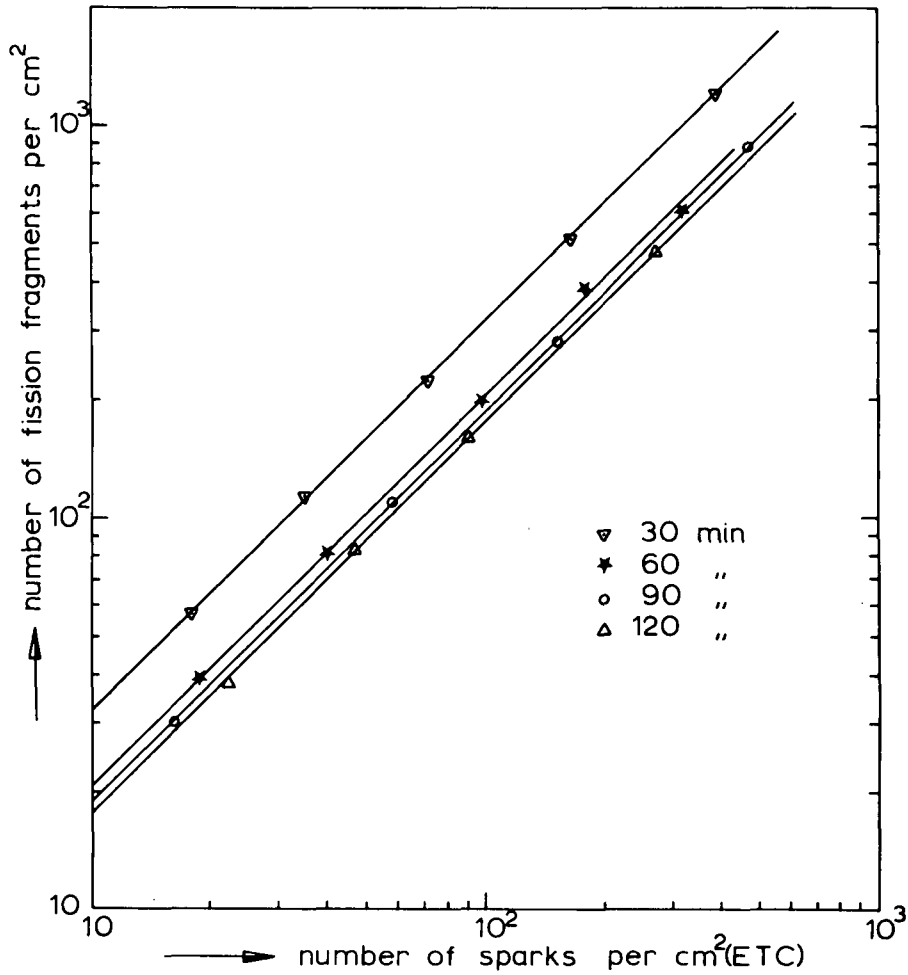

Fig. V.4 The efficiency of the ETC as a function of the etching time.

Pu : 98.358 percent ^{239}Pu, 1.613 percent ^{240}Pu, 0.029 percent ^{241}Pu and < 0.0005 percent ^{242}Pu

Np : 100 percent ^{237}Np

U : natural uranium.

In the case of plutonium we can also use the spontaneous fission of the ^{240}Pu present in the sample for the determination of the ETC efficiency.

For the calculations the figures in Table V.2 were used.

Table V.2 The half-lives of the different fissile materials.

Fissile material	$T_{\frac{1}{2}}$ (year)	
	α-decay	fission decay
^{239}Pu	2.44×10^{4}	5.5×10^{5}
^{240}Pu	6.6×10^{3}	1.17×10^{11}
^{242}Pu	3.8×10^{5}	7.06×10^{10}
^{237}Np	2.14×10^{6}	$> 4 \times 10^{16}$
^{234}U	2.50×10^{5}	2×10^{16}
^{235}U	6.96×10^{8}	1.9×10^{17}
^{238}U	4.50×10^{9}	7.19×10^{15}

References Wa 67 and Sc 68.

For the different fissile materials the efficiency of the ETC has been determined up to track densities of 10^{4} tracks per cm^{2} (figure V.5).
This was done in the following ways:

a) the spontaneous fission of the ^{240}Pu present in the plutonium sample.
b) the spontaneous fission of an electroplated ^{252}Cf source. The results obtained with the ^{252}Cf sample and the ^{240}Pu sample were in excellent agreement. This means that no appreciable fraction of the fission fragments are absorbed in the 0.1 mg per cm^{2} Pu layer. Because of the fact that the U and the Np samples have the same layer thickness as the Pu sample, we concluded that the ETC efficiency is equal for our samples of these three elements.

c) absolute measurements with a 15.6 MeV neutron generator. The absolute neutron flux was determined with aluminium samples: $^{27}Al(n,\alpha)^{24}Na$. The neutron cross section for this reaction was taken as 97 ± 5 mb. The absolute ^{24}Na activity was determined with the same calibrated NaI(Tl) well-type crystal. We noticed that the ETC efficiency determined with this method was about 1.6 times lower

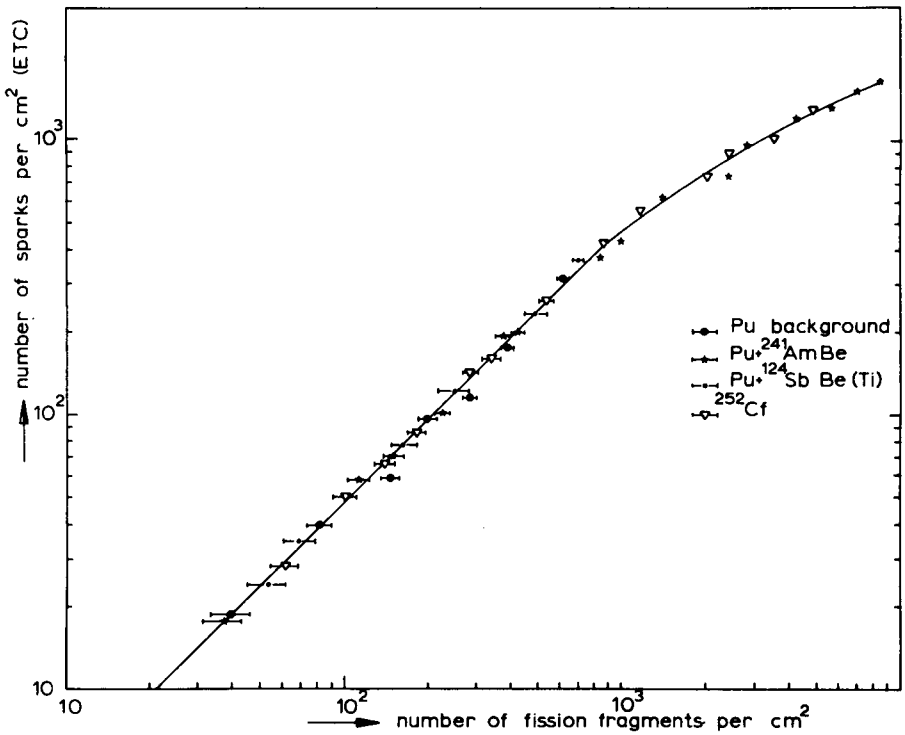

Fig. V.5 The efficiency of the ETC for an etching time of 60 minutes.

than the ETC efficiency obtained by methods a) and b). We noticed that in the forward direction neutron fission is registered with greater efficiency than in the backward direction. This was found to be dependent on the neutron

energy. For different neutron energies, up to 10 MeV, we determined the ratio of neutron fission registered in the forward direction to neutron fission registered in the backward direction:

$$\frac{\varepsilon_{F(E)}}{\varepsilon_{B(E)}} \qquad \text{V.1}$$

We assumed that the sum of the number of fission fragments registered in the forward direction and the number of fission products registered in the backward direction, divided by two, corresponds to the spontaneous fission efficiency, determined by methods a) and b). Or in an equation:

$$\frac{\varepsilon_{F(E)} + \varepsilon_{B(E)}}{2} = \varepsilon_{S.F.} \qquad \text{V.2}$$

With equations V.1 and V.2 we could determine the ETC efficiency for the U, the Np and the Pu samples. Investigations are still in progress to explain this anisotropy in the registration of fission fragments.

d) plutonium measurements with the calibrated ^{124}SbBe(Ti) neutron source. From equation VI.4 the real number of fission products was calculated. For the 21.0 keV neutrons a fission cross section of 1700 mb was used. After correcting for the anisotropy, in the fragment registration (which is very small in this case), the ETC efficiency was determined. Methods a), b) and d) agree very well. We also can say that we determined the Pu(n,f) cross section value at 21.0 keV. The value is put in Table VI.1.

e) relative plutonium measurements with the ^{241}AmBe neutron source. Irradiations of different length were performed to establish the ETC efficiency at very high track densities. With the help of methods a), b) and d) the absolute ETC efficiency curve could be determined up to track densities of 10^4 tracks per cm^2.

CHAPTER VI

EXPERIMENTAL RESULTS

As mentioned before, the measurements with the ^{124}SbBe neutron sources were carried out to check our neutron cross section evaluation at 21 - 22 keV.

The measurements with the ^{252}Cf neutron source gave us only an idea about the ^{115}In(n,n')^{115m}In and the ^{197}Au(n,2n)$^{196g+m}$Au cross section curves, for reasons mentioned later.

Mijnheer (Mij 70) has calibrated the different neutron sources by means of the well-known manganese sulphate bath method. He has also determined the anisotropy factors of these sources, which are very important for the calculation of the average cross section value ($\langle\sigma\rangle_{exp}$, equation II.6). The calibrations as well as the anisotropy factors of the neutron sources will be discussed in his thesis.

In order to reduce possible scattering of neutrons from the walls and the ground, the experiments were done in the open at an elevation of about 10 metres and far from any building. The neutron detector and the neutron source concerned were held by a small aluminium frame, which allowed accurate distance determination. The measurements were done at different distances from the source in the plane of symmetry perpendicular to the cylindrical axis of the source. The following relation was checked:

$$(T - S)\ (R - \Delta)^2 = C \qquad \text{VI.1}$$

in which T is the measured radioactivity corrected for decay or the number of tracks, counted by the ETC, produced per unit time; R is the real distance between the center of the source and the center of the neutron detector; S is the ac-

tivity or the number of tracks, due to scattered neutrons; Δ is a distance correction and C is a measure of the average cross section, which should be constant at various distances.

The factor $(R - \Delta)$ is the so-called "effective distance".

In our experimental position the distance between the neutron detector and the neutron source is small (maximum 30 cm for the gold and indium measurements, and maximum 8 cm for the neutron fission experiments). We can therefore assume that scattering of neutrons by air and by the small aluminium platform, is negligible, and we take $S = 0$.

Equation VI.1 now becomes:

$$T(R - \Delta)^2 = C \qquad \text{VI.2}$$

The values of C and Δ were calculated by means of a least square fit computer program, in which $\frac{1}{\sqrt{T}}$ was plotted against R.

It seemed that in the case of the gold and indium measurements the quantity Δ was negligible, whereas in the case of the neutron fission experiments the value of Δ was about - 3.5 mm for all neutron sources. Presumably this is due to the fact that our neutron sources are not actually point sources. The absolute distance R between the center of the neutron source and the center of the very thin plane neutron fission detectors is smaller than the "effective distance". This would suggest that for larger neutron sources the quantity Δ should become more negative. However, this is not seen to be the case. The value of Δ is about the same in all our experiments.

In the second place the angle, under which the detector actually "sees" the source, changes appreciably at short distances (0 - 8 cm). This "solid angle effect" will give a negative value of Δ. In the case of the gold and indium spheres, for which the distance between the detector and the source is much larger (15 - 30 cm) the detector always

"sees" the source under a very small angle. For this reason short distance measurements with gold and indium spheres were carried out as well.

However, experiments carried out at distances very close to the neutron source actually lead to inhomogeneities in the distribution of activity over the spheres. This will give a positive value of Δ.

Apparently the source size, the angle and the inhomogeneous activity will compensate each other in the gold and indium measurements.

The equations used to calculate the average cross section ($\langle\sigma\rangle_{exp}$) were:

$$\frac{T}{\varepsilon} = N. \frac{\Phi}{4\pi(R - \Delta)^2} K.\langle\sigma\rangle_{exp}(1 - e^{-\lambda t}) \qquad \text{VI.3}$$

in the case of the activation detectors gold and indium, and:

$$\frac{T_f}{\varepsilon_f} = N. \frac{\Phi}{4\pi(R - \Delta)^2}.K.\langle\sigma\rangle_{exp}t \qquad \text{VI.4}$$

in the case of the neutron fission detectors plutonium, neptunium and uranium, in which K is the anisotropy factor of the neutron source, Φ the total number of neutrons per second and ε and ε_f the detection efficiencies.

These expressions are the variations of equations II.1 and II.2.

In the case of the ^{124}SbBe measurements with gold, indium and plutonium a correction factor of 0.95 ± 0.02 is introduced into the above mentioned equations to account for the 380 keV neutrons.

The average neutron cross sections for the different sources.

For the various neutron sources the average neutron cross section ($\langle\sigma\rangle_{exp}$) was calculated with the help of the equations V.3 and V.4 respectively.

The values are summarized in Table VI.1.

In the same Table the calculated average neutron

cross sections for a ^{235}U and the ^{252}Cf neutron fission spectrum (T = 1.39 ± 0.03) have been given.

For the ^{235}U neutron fission spectrum the equation $N(E) = 0.484\ e^{-E} \sin h\sqrt{2E}$ was used (Wa 52).

From the indium measurements with the Mock-Fission neutron source it can be concluded that this source resembles a $^{226}RaBe$ source more closely than a Mock-Fission source does of the type studied by Tochilin (To 58).

Even the spectra of Tochilin (To 58) are not actually fission spectra, as is seen from Table VI.1. Thus our Mock-Fission source turned out to be of little interest. Other cross section measurements were not performed with this source.

As a first approximation the assumption can be made that the $^{9}Be(\alpha,n)$ spectra of the $^{241}AmBe$, the $^{239}PuBe$, the $^{242}CmBe$ and the $^{226}RaBe$ sources are about equal above 1.5 MeV.

In spite of the fact that the majority of neutron originating from the $^{9}Be(\alpha,n)$ reaction have energies above 1.5 MeV, neutrons of energies below 1.5 MeV provide the larger part of the activity due to the (n,γ) reaction, because the (n,γ) cross section values of ^{115}In and ^{197}Au are much higher below 1.5 MeV. For this reason the average cross section values for these reactions may be used to determine the number of neutrons below 1.5 MeV.

The average $^{115}In(n,\gamma)$ and $^{197}Au(n,\gamma)$ cross section values are highest for the $^{226}RaBe$ source. This means that the $^{226}RaBe$ source contains more neutrons with energies below 1.5 MeV than in the case for the $^{239}PuBe$, the $^{242}CmBe$ or the $^{241}AmBe$ source.

The average cross section for the $^{115}In(n,n')$ reaction has a lower value for the $^{226}RaBe$ source than for the $^{239}PuBe$, the $^{242}CmBe$ and the $^{241}AmBe$ source, which leads to the same conclusion.

Also the same conclusions could be drawn from the Pu(n,f), Np(n,f) and U(n,f) cross section values.

In Table I.2 the maximum neutron energies for the

$^{9}Be(\alpha,n)$ sources are summarized.

From the average cross section values for the $^{197}Au(n,2n)$ reaction we may draw conclusions concerning the upper part of the neutron spectrum (above 8.1 MeV). In Table VI.1 the values for the $^{242}CmBe$ and the $^{226}RaBe$ source are the highest ones, which means that these sources contain either neutrons with energies higher than the other $^{9}Be(\alpha,n)$ sources, or more neutrons above the $^{197}Au(n,2n)$ threshold energy. The average $^{197}Au(n,2n)$ cross section values from Table VI.1 can be related to the maximum neutron energy of the $^{9}Be(\alpha,n)$ spectra summarized in Table I.2.

The experimental average cross section values for the $^{115}In(n,n')$ and the $^{197}Au(n,2n)$ reaction for the ^{252}Cf neutron fission source are in good agreement with the calculated ones. In Chapter III it was mentioned that on the basis of the ^{252}Cf spectrum (equation I.1 with $T = 1.39 \pm 0.03$) it might have been concluded that the renormalized $^{115}In(n,n')$ reaction cross section curve and the $^{197}Au(n,2n)$ cross section curve of Tewes (Te 60) are correct. Otherwise, with the help of the correct $^{197}Au(n,2n)$ cross section curve, the $^{196g+m}Au$ activity can be used to calculate the T-value. From our experimental value $\langle\sigma\rangle_{exp} = 4.93 \pm 0.14$, and assuming an uncertainty in the excitation curve of 10 percent, a T-value of 1.39 ± 0.02 can be calculated for the upper part of the ^{252}Cf spectrum.

However, the $^{197}Au(n,\gamma)$ values deviate by a factor of about 1.25. From these values it can be concluded that the ^{252}Cf neutron spectrum is softer than equation I.1 suggests.

In this connection it should be taken into account that the ^{252}Cf material has been encapsuled by a monel container. The total neutron scattering cross section of monel increases rapidly with decreasing energy (from 3 barn at 1.0 MeV to 10 barn at 0.05 MeV). Single and multiple neutron scattering will take place inside the capsule. By a single elastic scattering process the neutrons lose only up to 4 percent of their primary energy, but with a monel thickness

Table VI.1 The average neutron cross sections

Source	neutron cross section (mb)				
	In(n,γ)	In(n,γ)+^{10}B	In(n,n')	In(n,n')+^{10}B	Au(n,γ)
^{241}AmBe	70.6 ± 4.0	60.7 ± 2.6	272 ± 15	258 ± 16	51.7 ± 1.1
^{239}PuBe	83.4 ± 3.1	77.0 ± 3.0	260 ± 10	234 ± 11	68.3 ± 1.5
^{226}RaBe	87.9 ± 3.9	82.3 ± 3.7	217 ± 17	227 ± 17	85.9 ± 2.8
^{242}CmBe	74.7 ± 2.7	67.9 ± 2.5	237 ± 9	226 ± 9	70.8 ± 1.7
Mock-Fission	96.4 ± 8.4	93.0 ± 6.3	252 ± 19	229 ± 28	n.m.
To 58 A	149 ± 15		168 ± 17		
B	137 ± 14		188 ± 19		
C	132 ± 13		195 ± 20		
^{235}U	134 ± 13		181 ± 18		
^{241}AmLi	264 ± 16	167 ± 13	-	-	237.8 ± 7.0
Be 65	224 ± 22	174 ± 17	-	-	232 ± 23
Ge 70b	208 ± 21	170 ± 17	-	-	201 ± 20
^{241}AmAl	162 ± 6	152 ± 11	118 ± 7	111 ± 13	116 ± 8
^{124}SbBe(Al)	550 ± 50	315 ± 30	-	-	655 ± 40
^{124}SbBe(Ti)	640 ± 40	325 ± 20	-	-	715 ± 30
^{252}Cf(exp)	125.3 ± 4.3	118.9 ± 4.5	188 ± 8	175 ± 7	95.5 ± 2.3
^{252}Cf(cal)	125 ± 13	115 ± 12	187 ± 19*	176 ± 18*	76 ± 7

* based on the renormalized ^{115}In(n,n')^{115}In cross section curve

for the different sources

neutron cross section (mb)					
$Au(n,\gamma)+^{10}B$	$Au(n,2n)$	$Au(n,2n)+^{10}B$	$Pu(n,f)$	$Np(n,f)$	$U(n,f)$
47.6 ± 1.3	37.6 ± 0.8	30.8 ± 0.7	1835 ± 60	1500 ± 45	490 ± 20
57.4 ± 1.3	29.6 ± 0.6	24.9 ± 0.6	1790 ± 60	1375 ± 40	455 ± 15
69.6 ± 2.4	40.9 ± 1.2	35.0 ± 1.4	1750 ± 60	1275 ± 50	365 ± 20
58.6 ± 1.5	40.2 ± 1.0	35.1 ± 1.0	1820 ± 60	1500 ± 60	495 ± 25
n.m.	n.m.	n.m.	n.m.	n.m.	n.m.
166.5 ± 4.6	-	-	1565 ± 160	400 ± 45	-
172 ± 17	-	-	1565 ± 160	410 ± 40	-
154 ± 15	-	-	1590 ± 160	560 ± 50	-
91 ± 12	-	-	1700 ± 200	710 ± 100	200 ± 40
380 ± 25	-	-	n.m.	-	-
380 ± 15	-	-	1700 ± 200	-	-
83.1 ± 2.1	4.93 ± 0.14	4.56 ± 0.14	1800 ± 60	1260 ± 60	310 ± 25
67 ± 7	5.0 ± 0.6	4.7 ± 0.5	1790 ± 180	1355 135	310 ± 30

of 0.45 cm the number of scattered neutrons above 1.0 MeV is 12 percent, increasing up to 34 percent at 0.05 MeV. This means that the ^{252}Cf neutron fission spectrum will shift slightly towards the low energy side. The change will be largest below 1.0 MeV. However, the change in the activation of gold by the (n,γ) process amounts to only 1 percent, which is not enough to account for the differences of 25 percent shown in Table VI.1.

Meadows (Me 67) concluded that the Maxwellian distribution fits the ^{252}Cf spectrum very well above 0.5 MeV, but that experimentally the total number of neutrons below 0.5 MeV is about 25 percent higher and that below 0.1 MeV there is an extra yield of neutrons of 2 percent not indicated by equation I.1 ($T = 1.39 \pm 0.03$). This means that the calculated cross section value for the $^{197}Au(n,\gamma)$ reaction will increase by about 20 percent in agreement with our experiments and the $^{115}In(n,\gamma)$ and the Pu(n,f) values with about 5 percent. The calculated cross section values for the reactions $^{115}In(n,n')$, $^{197}Au(n,2n)$, Np(n,f) and U(n,f) will be lowered by about 4 percent (still assuming a T-value of 1.39 ± 0.03).

However, the T-value of 1.565 (Table I.6), measured by Meadows is rather high in comparison to other measurements ($T = 1.39$).

The next explanation solved the discrepancy about the ^{252}Cf neutron spectrum.

As it will be shown later, the renormalized $^{115}In(n,n')$ cross section curve should be raised by 13 percent. This means that the calculated cross section value for the $^{115}In(n,n')$ reaction becomes 210 ± 21 (instead of 187 ± 19), no longer in agreement with the measured value of 188 ± 8 (10 percent lower).

From Table VI.1 it can also be seen that the measured Np(n,f) cross section value is about 7 percent lower than the calculated one. If we now assume that the renormalized

reaction cross section curves are correct, we have to change the ^{252}Cf neutron spectrum in such a way that the measured and calculated cross section values are in agreement. The only change we had to make is a flattening of the neutron spectrum below 2 MeV in such a way that the total number of neutrons below 2 MeV still remains constant.

It is further assumed that above 2 MeV the Maxwellian distribution with a T-value of 1.39 ± 0.03 is correct for the ^{252}Cf neutron spectrum. A flattening of the neutron spectrum below 2 MeV has no effect on the calculation of the average $^{115}In(n,\gamma)$ and the average Pu(n,f) cross section values, because both cross section curves are about constant between 150 keV and 1.5 MeV. Because of the fact that the $^{197}Au(n,\gamma)$ cross section curve rises very strongly below 2 MeV, the calculated cross section values will become higher and more in agreement with our measured values. The calculated $^{115}In(n,n')$, and Np(n,f) cross section values will become lower, whereas the U(n,f) and $^{197}Au(n,2n)$ cross section values will remain constant.

The uncertainty in the theoretical cross section values for the ^{252}Cf neutron spectrum was calculated on the basis of the uncertainties of the cross section curves, of the neutron scattering by the monel container and of the T-value (1.39 ± 0.03).

For the $^{241}AmLi$ source the average $^{115}In(n,\gamma)$ and the average $^{197}Au(n,\gamma)$ cross section values, calculated for the spectrum of Bennett (Be 65) and Geiger (Ge 70b), are given in Table VI.1. It is clear that our $^{241}AmLi$ values are in better agreement with those of Bennett.

From the values of the $^{241}AmAl$ source it can be concluded that the neutron spectrum is harder than that of $^{241}AmLi$, but softer than the ^{252}Cf neutron spectrum.

The average cross section values for the $^{124}SbBe$ sources tell us that the neutron spectrum of the $^{124}SbBe(Ti)$ source is somewhat softer than that of the $^{124}SbBe(Al)$ source.

The neutron transmission factors for the 2.2 g per cm^2 ^{10}B sphere and the different sources.

From Table VI.2 it can be seen that the experimental transmission factor for the ^{124}SbBe(Al) source is in agreement with the calculated one (equation III.2). However, the factor for the ^{124}SbBe(Ti) source is slightly lower than calculated, due to the uncertainty of the neutron spectrum of this source. It is difficult to calculate the transmission factor of this source, because of the very high total cross section of the titanium capsule around the antimony beryllium mixture (see Chapter I).

The experimental ^{115}In(n,γ) transmission factor for the ^{252}Cf source agrees well with the calculated value. However, the ^{197}Au(n,γ) value is somewhat lower than expected. This supports the suggestion that the ^{252}Cf spectrum below 1.0 MeV might be softer than equation I.1 (T = 1.39±0.03) indicates.

Within the accuracy of our measurements the transmission factors of the ^{115}In(n,γ) reaction are about equal for the ^{241}AmBe, the ^{239}PuBe, the ^{242}CmBe, the ^{226}RaBe, the Mock-Fission and the ^{252}Cf source. We would expect that a neutron source, which has more neutrons below 1.0 MeV than another source, would have a lower transmission factor. The explanation for this fact is that the ^{115}In(n,γ) reaction cross section has about the same value between 150 keV and 1.5 MeV and that the transmission factor does not change much in that energy range (see Table III.2).

In principle there must of course be a difference between the transmission factors for the various sources, but the statistical uncertainty in the measurements is too large to observe such details.

The ^{197}Au(n,γ) cross section curve follows a course which is quite different from that of the ^{115}In(n,γ) curve. Table VI.2 shows striking differences in the transmission factors for the various ^{9}Be(α,n) sources. For the ^{9}Be(α,n) sources the ^{226}RaBe source has the lowest transmission fac-

Table VI.2 The neutron transmission factors for the 2.2 g per cm^2 ^{10}B sphere and the different sources

Source	neutron transmission factors			
	$^{115}In(n,\gamma)$	$^{115}In(n,n')$	$^{197}Au(n,\gamma)$	$^{197}Au(n,2n)$
$^{241}AmBe$	0.860 ± 0.049	0.951 ± 0.068	0.922 ± 0.020	0.827 ± 0.013
$^{239}PuBe$	0.922 ± 0.030	0.901 ± 0.041	0.840 ± 0.012	0.843 ± 0.012
$^{226}RaBe$	0.936 ± 0.046	1.05 ± 0.11	0.809 ± 0.031	0.856 ± 0.035
$^{242}CmBe$	0.909 ± 0.027	0.957 ± 0.018	0.827 ± 0.019	0.872 ± 0.022
Mock-Fission	0.96 ± 0.11	0.91 ± 0.13	n.m.	n.m.
$^{241}AmLi$	0.635 ± 0.061	-	0.700 ± 0.027	-
$^{241}AmAl$	0.942 ± 0.077	0.94 ± 0.12	0.79 ± 0.11	-
$^{124}SbBe(Al)$ exp	0.57 ± 0.08	-	0.58 ± 0.04	-
$^{124}SbBe(Al)$ theor	0.56	-	0.56	-
$^{124}SbBe(Ti)$ exp	0.510 ± 0.018	-	0.526 ± 0.014	-
$^{124}SbBe(Ti)$ theor	0.54	-	0.54	-
^{252}Cf (exp)	0.949 ± 0.027	0.932 ± 0.034	0.871 ± 0.018	0.927 ± 0.024
^{252}Cf (theor)	0.92	0.94	0.91	0.94

tor for the $^{197}Au(n,\gamma)^{198}Au$ reaction. The conclusion to be drawn from this is that among the $^{9}Be(\alpha,n)$ sources the $^{226}RaBe$ source has the largest fraction of neutrons with energies below 1.5 MeV. On the same basis this fraction should be smallest in the $^{241}AmBe$ source of all $^{9}Be(\alpha,n)$ sources.

The transmission factors for the $^{115}In(n,n')$ reaction have essentially the same value for all sources. The reaction threshold energy is about 1.0 MeV and it was mentioned in Chapter III that above this energy value the transmission factor becomes constant.

However, the transmission factor values for the $^{197}Au(n,2n)$ reaction (threshold energy 8.1 MeV) are much lower than those for the $^{115}In(n,n')$ reaction, but constant. Calculations show that for a 2.2 g per cm^2 ^{10}B sphere the neutrons lose on the average about 17 percent of their primary energy when they scatter elastically. The number of neutrons that undergo elastic scattering is about 20 percent. This means that for the $^{9}Be(\alpha,n)$ sources most of the neutrons with energies above the $^{197}Au(n,2n)$ reaction threshold energy, which undergo elastic scattering, will enter the energy range below the reaction threshold energy for this process. In this case equations III.1 and III.2 are not valid anymore. We now have to calculate the transmission factor with the help of the total cross section value of $^{10}B(\sigma_t^B)$. The equation for the transmission factor becomes here:

$$T = e^{-\sigma_t^B N^B}$$

For the 2.2 g per cm^2 ^{10}B sphere we calculated from this equation a transmission factor value of 0.83 ± 0.04 in perfect agreement with the values shown in Table VI.2 for the $^{197}Au(n,2n)$ reaction.

However, the $^{197}Au(n,2n)$ transmission factor for the ^{252}Cf neutron source is more in agreement with the value calculated from equation III.2. This means that in contrary to the $^{9}Be(\alpha,n)$ neutron spectra the ^{252}Cf neutron spec-

trum extends far above 10 MeV, and that the number of elastic scattered neutrons, which enter the energy range below the $^{197}Au(n,2n)$ reaction threshold energy (8.1 MeV), is negligible.

From the measured $^{115}In(n,\gamma)$ and the measured $^{197}Au(n,\gamma)$ transmission factors for the $^{241}AmLi$ source, it can be concluded with the help of Table III.2 that the average neutron energy of this source lies below 100 keV.

From the transmission factors it can also be concluded that the $^{241}AmAl$ neutron spectrum is harder than that of $^{241}AmLi$, but softer than that of ^{252}Cf.

The fraction of neutrons below 1.5 MeV for the $^{9}Be(\alpha,n)$ sources and the ^{252}Cf source.

In Table VI.3 our results, calculated with the equations II.8 and II.11, are compared with the literature values.

For the $^{115}In(n,\gamma)$, the $^{115}In(n,\gamma) + {}^{10}B$ and the Pu(n,f) reaction, the value for $\langle\sigma\rangle_{<1.5}$ was taken as 170 mb, 155 mb and 1550 mb respectively.

The fraction of neutrons below 1.5 MeV for the different sources, calculated on the basis of the $^{115}In(n,\gamma)$, the Pu(n,f) and the U(n,f) measurements, agree well for the different neutron spectra.

It was quite surprising that the ratio

$$\frac{\int_{1.5}^{\infty} \phi(E)\ \sigma(E)\ dE}{\int_{1.5}^{\infty} \phi(E)\ dE}$$

used in eqaution II.11 is about constant for the published spectra of one type. For the $^{241}AmBe$ source, only the neutron spectrum of Greiss (Gr 68b) is rather different from the

Table VI.3 The fraction of neutrons below 1.5 MeV for the $^{9}Be(\alpha,n)$ sources and the ^{252}Cf source.

Source			fraction of neutrons below 1.5 MeV				
		literature		our results			
	Ci	author	fraction below 1.5 MeV	In(n,γ)	In(n,γ) + ^{10}B	Pu(n,f)	U(n,f)
$^{241}AmBe$	3	Cl 69	-	0.25	0.22	0.23	0.25
	0.74	Ge 64	0.17	0.27	0.24	0.23	0.26
	0.74	Ge 70a	0.17	0.25	0.21	0.24	0.24
	10	Gr 68b	-	0.20	0.17	0.21	0.22
	1	Kl 69	0.153	0.25	0.21	0.18	0.23
	0.1	Th 65	-	0.26	0.22	0.22	0.27
	1	Zi 69	0.155*				
	-	Zw 68	0.16	0.27	0.24	0.20	0.24
$^{239}PuBe$	5	Ak 63	-	0.33	0.34	0.30	0.29
	5	An 63	-	0.33	0.34	0.35	0.30
	-	Go 67	0.28	0.34	0.34	0.35	0.31
	2.8	Gr 67	-	0.32	0.32	0.34	0.30
	5	Hu 62	-	0.32	0.32	0.33	0.30
	5	Le 68	-	0.34	0.34	0.29	0.28
	-	Zw 68	0.12	0.35	0.36	0.33	0.30
$^{226}RaBe$	0.5	Ge 64	0.40	0.38	0.40	0.38	0.43
	-	Go 67	0.43	0.36	0.38	0.42	0.43
	0.2	Kl 69	0.33	0.39	0.41	0.38	0.43
	-	Ku 67	0.38	0.35	0.38	0.37	0.42
	0.2	Zi 69	0.345*				
$^{242}CmBe$	1	Lo 70	-	0.26	0.26	0.25	0.21
Mock-Fission	1	Go 67		0.35 ± 0.07		n.m.	n.m.
^{252}Cf	$8x10^{-4}$	T=1.39	0.46	0.48	0.530	0.48	0.46

* fraction of neutrons below 1.0 MeV

^{241}AmBe spectra determined by the other investigators. For this spectrum a very different value is calculated for this factor.

It was mentioned in Chapter II that the neutron spectrum above about 2 MeV is independent on the source size.

For this reason the data given in Table V.3 are only valid for the sources we used, the dimensions and other characteristics of which are given in Table I.1.

For the sources we used, ^{241}AmBe (3 Ci), ^{239}PuBe (5 Ci), ^{226}RaBe (0.1 Ci), ^{242}CmBe (1 Ci) and ^{252}Cf (8 x 10^{-4} Ci) no literature values are available.

The uncertainties in the ^{115}In(n,γ), ^{115}In(n,γ) + ^{10}B and Pu(n,f) data are 10 percent, based on the uncertainties of the neutron spectra above 1.5 MeV and the uncertainties of the cross section curves. The uncertainty in the U(n,f) data is 0.05 based on the same uncertainties mentioned above.

From the ^{252}Cf data it can be concluded that the measured fraction of neutrons below 1.5 MeV is in reasonable agreement with the calculated one.

It is possible that the fraction of neutrons below 1.5 MeV, given for our Mock-Fission source, is wrong. For the calculation of equation II.11, the ^{210}PoBe spectrum of Goryachev (Go 67) was used, whereas it was assumed that the Mock-Fission spectrum and the ^{210}PoBe spectrum of Goryachev were identical above 1.5 MeV.

The fraction of neutrons above the reaction threshold energies of ^{115}In(n,n'), U(n.f) and ^{197}Au(n,2n).

For the calculation of the fraction of neutrons above the reaction threshold energies, equation II.8 was used. The calculations were made for the different literature spectra, summarized in Table VI.3.
Only the average values are given in Table VI.4.

For the U(n,f) and the ^{197}Au(n,2n) reaction the calculation could be carried out easily, because the neutron spectra above 1.5 MeV are known very well.

Table VI.4 The fraction of neutrons above the reaction threshold energies of $^{237}Np(n,f)$, $^{115}In(n,n')$, U(n,f) and $^{197}Au(n,2n)$.

Source	fraction of neutrons above the reaction threshold energy			
	$^{237}Np(n,f)$	$^{115}In(n,n')$	U(n,f)	$^{197}Au(n,2n)$
	-0.5 MeV-	-1.0 MeV-	-1.5 MeV-	-8.1 MeV-
$^{241}AmBe$	0.86 ± 0.05	0.96 ± 0.10* 0.83 ± 0.08+	0.76 ± 0.05	0.092 ± 0.009
$^{239}PuBe$	0.79 ± 0.05	0.84 ± 0.08 0.73 ± 0.07	0.70 ± 0.05	0.086 ± 0.009
$^{226}RaBe$	0.77 ± 0.05	0.75 ± 0.08 0.65 ± 0.07	0.57 ± 0.05	0.082 ± 0.008
$^{242}CmBe$	0.87 ± 0.05	0.92 ± 0.09 0.80 ± 0.08	0.79 ± 0.05	0.077 ± 0.008
Mock-Fission	n.m.	0.81 ± 0.08 0.70 ± 0.10	n.m.	n.m.
$^{241}AmLi$	0.30 ± 0.04		-	-
Be 65	0.33 ± 0.03		-	-
Ge 70b	0.55 ± 0.05		-	-
$^{241}AmAl$	0.55 ± 0.08	0.40 ± 0.05 0.35 ± 0.05	0.40 ± 0.08	-
$^{252}Cf(exp)$	0.81 ± 0.06	0.70 ± 0.04 0.62 ± 0.04	0.54 ± 0.05	0.011 ± 0.001
$^{252}Cf(cal)$	0.867 ± 0.004	0.695 ± 0.0077	0.539 ± 0.010	0.01

* based on the renormalized cross section curve of $^{115}In(n,n')$

\+ based on the proposed cross section curve of $^{115}In(n,n')$

However, for the calculation of the fraction of neutrons above the threshold energies of Np(n,f) and ^{115}In(n,n'), we have extended many of the existing neutron spectra to the low energy part, assuming a neutron peak at 300 keV, due to the secondary reactions, described in Chapter I. The extension was carried out in such a way that the fraction of neutrons below 1.5 MeV was in agreement with the data given in Table VI.3.

For the ^{237}Np(n,f) and the ^{115}In(n,n') reaction the fraction of neutrons was calculated above 0.5 MeV and 1.0 MeV respectively. The energy values 0.5 MeV and 1.0 MeV are not the actual reaction threshold energies of the ^{237}Np(n,f) and the ^{115}In(n,n') reaction.

From Table VI.4 it can be seen that the ^{241}AmLi spectrum of Bennett (Be 65) is likely to be correct. For this source the fraction of neutrons above 1.0 MeV could not be determined, because no ^{115m}In activity was measured. Even no upper limit could be given.

In first approximation the fraction of neutrons above the ^{115}In(n,n') threshold energy for the different ^{9}Be(α,n) neutron sources, calculated with equation II.8 and based on the renormalized ^{115}In(n,n') cross section curve, was high, compared to the data based on the Np(n,f) and U(n,f) measurements (see Table VI.4). However, many published ^{9}Be(α,n) neutron spectra show that the fraction of neutrons above 1.0 MeV is about 0.05 higher than that above 1.5 MeV. The ^{115}In(n,n') data could only be brought into better agreement if we raised the ^{115}In(n,n') cross section curve with 13 percent.

The proposed ^{115}In(n,n') cross section curve is given as a dashed line in figure III.4.

For the renormalization of the ^{115}In(n,n') cross section curve it was assumed that the 335 keV γ-ray of ^{115m}In accompanies 50.0 percent of the decays. For the absolute calibration of the ^{115m}In activity the same value was used.

For further neutron measurements with the help of the

$^{115}In(n,n')$ threshold detector, it should be advisable to solve the discrepancies between the different published $^{115}In(n,n')$ cross section curves first.

Heertje (He 63; He 64) determined for the $^{226}RaBe$ and the $^{239}PuBe$ sources we used, the fraction of neutrons below 1.0 MeV, mainly with the help of the $^{115}In(n,n')$, $^{31}P(n,p)$ and $^{32}S(n,p)$ reactions. He noticed that for the $^{226}RaBe$ neutron source the fraction of neutrons below 1.0 MeV was at least 0.30, whereas for the $^{239}PuBe$ neutron source the fraction of neutrons was at least 0.25. These values are in good agreement with those we determined.

Average neutron energy below 1.5 MeV for the $^{9}Be(\alpha,n)$ sources.

It was already explained in Chapter II that with the help of the results of the $^{115}In(n,\gamma)$, the U(n,f) and the Pu(n,f) measurements, the average gold cross section value below 1.5 MeV could be calculated.

This procedure was carried out for the different $^{9}Be(\alpha,n)$ neutron spectra. With the help of the cross section curves of gold, shown in figure III.5, the average neutron energies below 1.5 MeV were determined.

The data are given in Table VI.5.

It is noticed that the gold measurements with and without the ^{10}B sphere lead to the same result.

It is also clear that the expectation of a 300 keV neutron peak in the $^{9}Be(\alpha,n)$ spectra is more or less verified in our measurements.

Except for the $^{242}CmBe$ spectrum, the average neutron energy values of the other $^{9}Be(\alpha,n)$ spectra tend to the conclusion that a neutron source with the largest fraction of neutrons below 1.5 MeV has the lowest average neutron energy. This can be understood very well if we assume that in the energy range 150 keV to 1.5 keV a monoenergetic neutron peak at 300 MeV exists, with a tail at the high energy part toward 1.5 MeV.

Table VI.5 actually shows that the tail in the ^{241}AmBe and ^{239}PuBe spectrum is more important than that in the ^{226}RaBe spectrum.

As was shown earlier, the ^{242}CmBe spectrum seems different from what is expected for ^{9}Be(α,n) sources. From the ^{242}CmBe data we can only say that the neutron spectrum below 1.5 MeV is rather soft, perhaps even a little softer than the ^{226}RaBe spectrum.

Table VI.5 Average neutron energy below 1.5 MeV for the ^{9}Be(α,n) sources.

Source	average fraction of neutrons below 1.5 MeV	average neutron energy (keV) ^{197}Au(n,γ)	^{197}Au(n,γ) + ^{10}B
^{241}AmBe	0.23	400 ± 40	375 ± 40
^{239}PuBe	0.33	375 ± 40	420 ± 40
^{226}RaBe	0.38	310 ± 30	360 ± 40
^{242}CmBe	0.25	270 ± 30	300 ± 30

SUMMARY

The main purpose of our investigations was to determine the neutron spectrum below 1.5 MeV of different kinds of $^{9}Be(\alpha,n)$ sources and of a ^{252}Cf source. The neutron spectra of an $^{241}AmLi$ and of an $^{241}AmAl$ were also determined

For our investigations we used simple neutron detectors. One type consists of gold and indium spheres, frequently surrounded by a layer of ^{10}B.

Besides gold and indium, thin layers of fissile materials were used in combination with plastic foils, which record the fission products as small tracks.

After a discussion, in Chapter I, of the energy spectra of the neutron sources used by us, Chapter II describes the aspects of neutron activation.

For our calculations very accurate reaction cross section curves were required. In Chapter III, the renormalization of the reaction cross section curves is discussed.

Chapter IV deals with the calibration of the neutron activation detectors.

For the determination of the number of fission fragments registered by the plastic foils an electrical track counter (ETC) was developed. The characteristics of the ETC and the use and calibration of the fission detectors are described in Chapter V.

Finally, the results are collected in Chapter VI. It is concluded that the excitation curve of the reaction $^{115}In(n,n')^{115m}In$, based on our renormalization, is not correct. This cross section curve was therefore changed to make it agree with our experiments.

We also confirmed the shape of the ^{252}Cf neutron spectrum in the energy range below 2 MeV. It was even possible with the help of the measured $^{196g+m}Au$ activity and the correct cross section curve of the reaction

$^{197}Au(n,2n)^{196g+m}Au$ (threshold energy 8.1 MeV) to determine the ^{252}Cf neutron spectrum at very high energies.

SAMENVATTING

Het hoofddoel van ons onderzoek was het bepalen van het neutronenspektrum beneden 1.5 MeV van verschillende $^{9}Be(\alpha,n)$ bronnen en een ^{252}Cf bron. De neutronen spektra van een $^{241}AmLi$ en van een $^{241}AmAl$ werden ook onderzocht.

Voor dit onderzoek werden eenvoudige neutronen detektoren gebruikt. Eén detektor bestond uit goud en indium bolletjes, al of niet omringd door een laag ^{10}B.

Naast goud en indium werden dunne lagen splijtingsmaterialen gebruikt in kombinatie met plastik folies, die de splijtingsprodukten registreren als kleine spoortjes.

Na een diskussie, in Hoofdstuk I, omtrent de energie spektra van de neutronen bronnen, door ons gebruikt, beschrijft Hoofdstuk II de aspekten van de neutronen aktivering.

Voor onze berekeningen waren zeer nauwkeurige reaktie cross section curves vereist. In Hoofdstuk III wordt de hernormering van de reaktie cross section curves beschreven.

Hoofdstuk IV behandelt de kalibratie van de neutronen aktiveringsdetektoren.

Voor het bepalen van het aantal spoortjes in de plastik folies werd een "electrical track counter (ETC)" ontwikkeld. De eigenschappen van de ETC en het gebruik en de kalibratie van de splijtingsdetektoren worden beschreven in Hoofdstuk V.

Tenslotte zijn de resultaten gegeven in Hoofdstuk VI. Hieruit kon gekonkludeerd worden dat de excitatie curve van de reaktie $^{115}In(n,n')^{115m}In$, gebaseerd op onze hernormering, niet juist is. Deze cross section curve werd zo veranderd dat onze experimenten beter overeenstemden.

We stelden ook de vorm vast van het ^{252}Cf neutronen spektrum in het energiegebied beneden 2 MeV. Het was zelfs mogelijk met behulp van de gemeten $^{186g+m}Au$ aktiviteit en

de juiste cross section curve van de reaktie $^{197}Au(n,2n)^{196g+m}Au$ (drempelenergie 8,1 MeV) het ^{252}Cf neutronen spektrum te bepalen bij zeer hoge energien.

REFERENCES

Ak 63	Akagi, H., Lehman, R.L.	Health Phys. 9, 207(1963)
An 63	Anderson, M.E., Bond, W.H.	Nucl.Phys. 43, 330(1963)
An 68	Anderson, M.E., Neff, R.A.	Trans.Am.Nucl.Soc.11,454(1968)
Ar 68	Arnold, E.D.	Eng.Comp.Rad.Sh. 1, 30(1968)
As 58	Ashby, V.J. et al.	Phys.Rev. 111, 616(1958)
Au 69	Auer, I.P.	Nucl.Phys. A124, 199(1969)
Ba 62	Basson, J.K., Dennis, J.A.	Nucl.Instr.Meth. 16, 321(1962)
Ba 64	Barry, J.F.	J.Nucl.Energy A/B18, 491(1964)
Be 56	Bethe, H.A., Beyster, J.R. and Carter, R.E.	J.Nucl.Energy 3,207, 273(1956) { J.Nucl.Energy 4, 3, 147(1956)
Be 65	Bennett, E.F.	ANL-7110 337(1965)
Be 66	Belanova, T.S., Van'kov,A.A.	J.Nucl.Energy A/B20, 411(1966)
Be 69	Bensch, F., Vesely, F.	J.Nucl.Energy 23, 537(1969)
Bo 61	Bonner, T.W.	Nucl.Phys. 23, 116(1961)
Br 67	Broadhead, K.G., Shanks,D.E.	J.Appl.Rad.Isot. 18, 279(1967)
Bu 67	Butler, J.P., Santry, D.C.	Bull.Am.Phys.Soc. 11(12), 547(1967)
Ch 65	Chaubey, A.K., Sehgal, M.L.	Nucl.Phys. 66, 267(1965)
Cl 69	Cloth, P., Hecker, R.	Nukleonik 12, 163(1969)
Co 48	Cohen, S.G.	Nature 161, 475(1948)
Co 61	Cox, S.A.	Phys.Rev. 122,1280(1961)
Co 64	Cox, S.A.	Phys.Rev. B133, 378(1964)
Co 65	Condé, H., During, G.	Ark.Phys. 29, 313(1965
Co 68	Colditz, J., Hill, P.	Anz.Oesterr.Akad.Wiss., Nath.Naturw.Kl. 10, 236(1968)
Cr 69	Cross, W.G., Tommasino, L.	Int.Top.Conf.Nucl.Tr.Reg. Ins.Sol.Appl. Clermont-Ferrand (1969)

Di 60	Diven, B.G., Terrell, J. and Hemmendinger, A.	Phys.Rev.	120, 556(1960)
Di 67	Diment, K.M.	AERE-R5224	(1967)
Fr 70	Fricke, M.P.	GA-10114	(1970)
Ge 64	Geiger, K.W., Hargrove, C.K.	Nucl.Phys.	53, 204(1964)
Ge 70a	Geiger, K.W.,Van der Zwan,L.	J.Appl.Rad.Isot.	21, 193(1970)
Ge 70b	Geiger, K.W.,Van der Zwan,L.	Joint Congress Can.Ass.Phys; Am.Ph.Soc;Soc.Mex.Fis.	(1970)
Go 67	Goryachev, I.V. et al.	Symp.Neutron Mon.Rad.Prot. Vienna	(1967)
Gr 55	Graves, E.R., Davis, R.W.	Phys.Rev.	97,1205(1955)
Gr 67	Gredel, H., Säbel, M.	Symp.Neutron Mon.Rad.Prot. Vienna	(1967)
Gr 68a	Grench, H.A., Menlove, H.O.	Phys.Rev.	165,1298(1968)
Gr 68b	Greiss, H.B.	Nukleonik	10, 283(1968)
Gr 69	Green, L.	Nucl.Sc.Eng.	37, 232(1969)
Gu 68	Gubernator, K., Moret, H.	EUR 3950e	(1968)
Ha 65	Harris, K.K. et al.	Nucl.Phys.	67, 37(1965)
Ha 68	Hankla, A.K., Hamilton, J.H. and Fink, R.W.	Bull.Am.Phys.Soc.	13,1421(1968)
Ha 69	Hart, W.	AHSB(S) R 169	(1969)
He 59	Hess, W.N.	Ann.Phys.	6, 115(1959)
He 63	Heertje, I.	Thesis, Univ. Amsterdam	(1963)
He 64	Heertje, I., Van Westen,N.P. and Aten Jr., A.H.W.	Physica	30,1846(1964)
Hu 62	Huber, P. et al.	Helv.Phys.Acta	35, 557(1962)
Iz 60	Izvakadnu	Nucl.Sc.Abstr.	14,3218(1960)

Ja 67	Jansen, J.W.F., Pauw, H.	Nucl.Phys.	A94, 235(1967)
Jo 59	Johnsrud, A.E., Silbert, M.G. and Barshall, H.H.	Phys.Rev.	116, 927(1959)
Kl 69	Kluge, H.	Z.Naturforsch.	24a,1289(1969)
Ko 67	Kooi, J., Mijnheer, B.J. and Aten, Jr., A.H.W.	Act.Rev.	1(1)(1967)
Ku 67	Kukhtevich, V.I., Trykov, L.A. and Trykov, O.A.	Symp.Neutron Mon.Rad.Prot. Vienna	(1967)
La 69	Lark, N.L.	Nucl.Instr.Methods	67,137(1969)
Le 68	Lehman, R.L.	Nucl.Instr.Methods	60,253(1968)
Lo 70	Lorch, E.	Private Communications	
Ma 54	Martin, H.G., Diven, B.C. and Taschek, R.F.	Phys.Rev.	93, 199(1954)
Ma 65	Mangel, S.U., Khurana,C.S.	Nucl.Phys.	69, 158(1965)
Ma 67	Mäcklin, R.L., Gibbons, J.H.	Phys.Rev.	159,1007(1967)
Me 67a	Menlove, H.O. et al.	Phys.Rev.	163,1299(1967)
Me 67b	Menlove, H.O. et al.	Phys.Rev.	163,1308(1967)
Me 67c	Meadows, J.W.	Phys.Rev.	157,1076(1967)
Me 69	Meyers, R.A.	Nucl.Phys.	A127, 595(1969)
Mi 62	Miskel, J.A. et al.	Phys.Rev.	128,2717(1962)
Mo 69	Moshkin, G.N., Tyufyakov,N.D. and Shtan, A.S.	At.Energ.	26, 384(1969)
Mij 70	Mijnheer, B.J.	Private Communications	
Na 66	Nagel, W.	Thesis, Univ. Amsterdam	(1966)
No 62	Notarrigo, S. et al.	Nucl.Phys.	29, 507(1962)
No 69	Notarrigo, S. et al.	Nucl.Phys.	A125, 28(1969)

Pa 53	Paul, E.B., Clarke, R.L.	Can.J.Phys.	31, 267(1953)
Pe 67	Petö, G., Miligy, Z. and Hunyadi, I.	J.Nucl.Energy	21, 797(1967)
Pe 68	Pearlstein, S.	Nucl.Data Sect.	A-3(3) (1968)
Po 68	Pönitz, W.P., Kompe, D. and Menlove, H.O.	J.Nucl.Energy	22, 505(1968)
Pr 61	Prestwood, R.J., Bayhurst,B.P.	Phys.Rev.	121,1438(1961)
Ro 62	St. Romain, F.A. et al.	Phys.Rev.	126,1794(1962)
Ru 68	De Ruyter, A.W.	Thesis, Univ. Amsterdam	(1968)
Ry 66	Ryves, T.B. et al.	J.Nucl.Energy	A/B20, 249(1966)
Ry 67	Ryves, T.B., Beale, D.W.	J.Appl.Rad.Isot.	18, 204(1967)
Sc 60	Schmidt, H.W.	Nucl.Phys.	20, 220(1960)
Sc 68	Schirmer, W., Wächter, N.	Act.Rev.	1, (2)(1968)
Sm 57	Smith A.B., Fields, P.R. and Roberts, J.H.	Phys.Rev.	108, 411(1957)
Te 60	Tewes et al.	Wash-1028	(1960)
Th 65	Thompson, M.N., Taylor, J.M.	Nucl.Instr.Methods	37,305(1965)
To 58	Tochilin, E., Alves, R.V.	Nucleonics	16(11), 145(1958)
To 63	Topp, S.V.	Trans.Am.Nucl.Soc.	6, 45(1963)
Ve 68	Verbinski, V.V. et al.	Phys.Rev.	170, 916(1968)
Vi 67	Vialettes, H.	Symp.Neutron Mon.Rad.Prot. Vienna	(1967)
Vo 68	Vonack, H.K. et al.	Nucl.Phys.	A118, 9(1968)
Wa 52	Watt, B.E.	Phys.Rev.	87,1037(1952)
Wa 67	Wapstra, A.H.	Act.Rev.	1(1) (1967)
Zi 69	Zill, H.	Z.Naturforsch.	24,1287(1969)
Zw 68	Van der Zwan, L.	Can.J.Phys.	46,1527(1968)